

ORIGINAL ARTICLE

Balance Between Rapid Delayed Rectifier K^+ Current and Late Na^+ Current on Ventricular Repolarization

An Effective Antiarrhythmic Target?

Bence Hegyi¹, MD, PhD; Ye Chen-Izu, PhD; Leighton T. Izu, PhD; Sridharan Rajamani, PhD; Luiz Belardinelli, MD; Donald M. Bers², PhD; Tamás Bányász³, MD, PhD

BACKGROUND: Rapid delayed rectifier K^+ current (I_{Kr}) and late Na^+ current (I_{NaL}) significantly shape the cardiac action potential (AP). Changes in their magnitudes can cause either long or short QT syndromes associated with malignant ventricular arrhythmias and sudden cardiac death.

METHODS: Physiological self AP-clamp was used to measure I_{NaL} and I_{Kr} during the AP in rabbit and porcine ventricular cardiomyocytes to test our hypothesis that the balance between I_{Kr} and I_{NaL} affects repolarization stability in health and disease conditions.

RESULTS: We found comparable amount of net charge carried by I_{Kr} and I_{NaL} during the physiological AP, suggesting that outward K^+ current via I_{Kr} and inward Na^+ current via I_{NaL} are in balance during physiological repolarization. Remarkably, I_{Kr} and I_{NaL} integrals in each control myocyte were highly correlated in both healthy rabbit and pig myocytes, despite high overall cell-to-cell variability. This close correlation was lost in heart failure myocytes from both species. Pretreatment with E-4031 to block I_{Kr} (mimicking long QT syndrome 2) or with sea anemone toxin II to impair Na^+ channel inactivation (mimicking long QT syndrome 3) prolonged AP duration (APD); however, using GS-967 to inhibit I_{NaL} sufficiently restored APD to control in both cases. Importantly, I_{NaL} inhibition significantly reduced the beat-to-beat and short-term variabilities of APD. Moreover, I_{NaL} inhibition also restored APD and repolarization stability in heart failure. Conversely, pretreatment with GS-967 shortened APD (mimicking short QT syndrome), and E-4031 reverted APD shortening. Furthermore, the amplitude of AP alternans occurring at high pacing frequency was decreased by I_{NaL} inhibition, increased by I_{Kr} inhibition, and restored by combined I_{NaL} and I_{Kr} inhibitions.

CONCLUSIONS: Our data demonstrate that I_{Kr} and I_{NaL} are counterbalancing currents during the physiological ventricular AP and their integrals covary in individual myocytes. Targeting these ionic currents to normalize their balance may have significant therapeutic potential in heart diseases with repolarization abnormalities.

VISUAL OVERVIEW: A visual overview is available for this article.

Key Words: action potential ■ Brugada syndrome ■ heart ■ long QT syndrome ■ tetrodotoxin

The shape of the cardiac action potential (AP) is determined by an integrative process between various depolarizing and repolarizing ionic currents. Pathological alterations in their balance may result in

either prolongation or shortening of AP duration (APD) manifested as long or short QT interval in the ECG.¹ The rapid delayed rectifier K^+ current (I_{Kr}) and the late Na^+ current (I_{NaL}) significantly affect AP repolarization, thus

Correspondence to: Bence Hegyi, MD, PhD, Department of Pharmacology, University of California, Davis, 451 Health Sciences Dr, Davis, CA 95616. Email bhegyi@ucdavis.edu

The Data Supplement is available at <https://www.ahajournals.org/doi/suppl/10.1161/CIRCEP.119.008130>.

For Sources of Funding and Disclosures, see page 347.

© 2020 American Heart Association, Inc.

Circulation: Arrhythmia and Electrophysiology is available at www.ahajournals.org/journal/circep



WHAT IS KNOWN?

- Rapid delayed rectifier K^+ current (I_{Kr} , hERG channels) and late Na^+ current (I_{NaL} , predominantly $Na_v1.5$ channels) are significant contributors to ventricular action potential duration.
- Changes in I_{Kr} and I_{NaL} magnitudes cause repolarization abnormalities such as long and short QT syndromes with increased risk of cardiac arrhythmias.

WHAT THE STUDY ADDS?

- I_{Kr} and I_{NaL} are in balance under the ventricular action potential, and their magnitude significantly correlate among cardiomyocytes to control action potential duration and its temporal variability (beat-to-beat variations and tachypacing-induced alternans).
- Rebalancing I_{Kr} and I_{NaL} in disease (long QT syndrome 2 and long QT syndrome 3, short QT) can effectively normalize repolarization.
- I_{Kr} and I_{NaL} are remodeled in ischemic and non-ischemic heart failure, their correlation is lost, and their balance is altered, leading to impaired repolarization.

Nonstandard Abbreviations and Acronyms

APD	action potential duration
ATX-II	sea anemone toxin II
BrS	Brugada syndrome
CaMKII	Ca^{2+} /calmodulin-dependent protein kinase II
–dV/dtmax	maximal rate of repolarization
hERG	human ether-a-go-go-related gene
IKr	rapid delayed rectifier K^+ current
I_{NaL}	late Na^+ current
LQT	long QT syndrome
SCN5A	sodium voltage-gated channel alpha subunit 5
SQT	short QT syndrome
STV	short-term variability

contributing to regulation of the APD.² Accordingly, both reduced I_{Kr} and increased I_{NaL} are known to cause long QT syndrome (LQT2 and LQT3, respectively), a clinical condition associated with increased risk for torsades de pointes-type ventricular tachycardia.² On the contrary, gain-of-function mutations in hERG (human ether-a-go-go-related gene; $K_v11.1$ channel, increased I_{Kr}) and loss-of-function mutations in SCN5A (sodium voltage-gated channel alpha subunit 5; $Na_v1.5$ channels, decreased I_{Na}) can lead to short QT syndrome (SQT) and Brugada syndrome.^{3,4}

Cellular electrophysiological^{5,6} and modeling studies^{7b} demonstrate that both I_{Kr} and I_{NaL} are activated during

phase 3 of the ventricular AP, and it has been proposed that I_{Kr} and I_{NaL} may counterbalance each other during physiological repolarization.^{7,9–11} However, this concept has not been systematically tested yet and supporting experimental data are sparse. Moreover, APD and plateau height are critical determinants of I_{Kr} and I_{NaL} densities and net charges under the AP.⁵ Consequently, APD prolongation may facilitate I_{Kr} and I_{NaL} accumulation during the AP, whereas I_{Kr} and I_{NaL} can be reduced when APD is shortened. Therefore, we aimed to compare the impact of I_{Kr} and I_{NaL} on ventricular repolarization in health and disease. Clinical findings also support such concept because treatments with mexiletine,^{12,13} ranolazine,¹⁴ and hydroquinidine,^{15,16} which may restore the balance between I_{Kr} and I_{NaL} can be beneficial in selected patients with LQT, SQT, and Brugada syndrome. We hypothesized that the I_{Kr}/I_{NaL} balance, as previously proposed,^{7,9–11} is a critical determinant of APD, and targeting this balance may represent a novel antiarrhythmic strategy.

We systematically measured APs and ionic currents in rabbit and porcine ventricular cardiomyocytes using physiological self AP-clamp technique¹⁷ in control, in pharmacologically-induced APD prolongation and shortening (modeling LQT and SQT), and in congestive heart failure (HF) induced by combined pressure/volume overload in rabbits¹⁸ and by chronic myocardial infarction in pigs.⁶ We also tested the relative contributions of I_{Kr} and I_{NaL} to the stability of APD in health and disease because the increased beat-to-beat and short-term variabilities of APD can be better predictors of cardiac arrhythmias than the steady-state APD alone.¹⁹ The mechanistic understanding of the relationship between I_{Kr} and I_{NaL} to set repolarization stability in cardiac health and disease may lead to more rational drug therapies.

METHODS

The data that support the findings of this study are available from the corresponding author upon reasonable request.

All animal handling and laboratory procedures were in accordance with the approved protocols (No. 20867 and No. 21137) of the local Institutional Animal Care and Use Committee conforming to the Guide for the Care and Use of Laboratory Animals published by the US National Institute of Health (Eighth edition, 2011). Chemicals and reagents were purchased from Sigma-Aldrich Co (St. Louis, MO) if not specified otherwise. GS-967 was obtained from Gilead Sciences, Inc (Foster City, CA), and E-4031 was from Tocris Bioscience (Bristol, United Kingdom).

Animal Models and Cell Isolation

Ventricular cardiomyocytes were isolated from 20 New Zealand White rabbits (male, 4-month-old) using a standard enzymatic technique with collagenase type II (Worthington Biochemical,

Co, Lakewood, NJ) and protease type XIV (Sigma-Aldrich), as previously described.²⁰

HF was induced in New Zealand White rabbits (male, 4-month-old) by aortic insufficiency and 4 weeks later by aortic constriction as previously described.^{18,21,22} Data here reported was obtained from 6 HF and 4 age-matched control (AM) rabbits. HF progression was monitored periodically by echocardiography. Cardiomyocytes were isolated from rabbits at 2 to 2.5 years of age when left ventricular end-systolic dimension exceeded 1.45 cm (detailed morphometric and echocardiography data are shown in Table I in the [Data Supplement](#)).¹⁸ Cardiomyocytes isolated from healthy AM rabbits were used in control experiments.

Yucatan mini-pigs (male, 4–6-month-old) were subjected to microbead embolization of the first diagonal branch of the left anterior descending coronary artery, which caused transmural myocardial infarction and progressive reduction in ejection fraction over 5 months (from the preoperative $68.1 \pm 3.9\%$ to $44.2 \pm 4.9\%$, $N=6$ animals, $P<0.01$), providing a clinically relevant large animal ischemic cardiomyopathy model as previously described.⁶ Cardiomyocytes were isolated from the remote zone of the infarct (>2 cm from the infarcted region) 5 months postmyocardial infarction. As control, cardiomyocytes were isolated from the same region of the heart of 4 healthy, age-matched sham control mini-pigs.

Electrophysiology

Recordings were performed in isolated ventricular cardiomyocytes using whole-cell patch-clamp with physiological solutions at $36 \pm 0.1^\circ\text{C}$ (for ionic composition, see [Data Supplement](#)). APs were evoked in current-clamp experiments where cells were stimulated with short suprathreshold depolarizing pulses at 1 to 5 Hz pacing frequencies delivered via the patch pipette. Fifty consecutive APs were recorded to examine the average behavior at each pacing frequency. Short-term variability (STV) of APD measured at 90% of repolarization (APD_{90}) was calculated according to the following formula: $\text{STV} = \frac{\sum(|\text{APD}_{i+1} - \text{APD}_i|)}{(n_{\text{beats}} - 1) \times \sqrt{2}}$, where APD_i and APD_{i+1} indicate the i^{th} and $(i+1)^{\text{th}}$ APD_{90} values, respectively, and n_{beats} denotes the number of consecutive beats analyzed.²³ Changes in STV are presented as Poincaré plots, where 50 consecutive APD_{90} values are plotted, each against the previous APD_{90} . To analyze further the variability of repolarization, the difference between consecutive APD_{90} values were grouped in milliseconds ranges, and the overall probability of their appearance was calculated in each cell. Then these data were plotted in cumulative distribution curves to illustrate the changes in beat-to-beat variability of APD_{90} .²⁴

Ionic currents during the AP were measured using self AP-clamp (at 2 Hz pacing in rabbits, and at 1 Hz in pigs) with physiological solutions, preserved $[\text{Ca}^{2+}]_i$ cycling, and sequential block of specific ionic currents using selective ion channel inhibitors (Table II in the [Data Supplement](#)), as previously described.^{6,17} A representative example is shown in Figure 1. E-4031 (1 $\mu\text{mol/L}$) and GS-967 (1 $\mu\text{mol/L}$) have been used to inhibit I_{Kr} and I_{NaL} , respectively.

Statistical Analysis

Data are expressed as mean \pm SEM. The number of cells in each experimental group was reported as n/N =number of cells/number of animals. Statistical significance of differences was evaluated using paired Student t test or ANOVA with Bonferroni post test as appropriate. Differences were deemed significant if $P<0.05$.

RESULTS

Profile of the Major Ionic Currents Under Physiological AP-Clamp

To assess the potential impact of I_{Kr} and I_{NaL} on AP repolarization, first, we recorded the major depolarizing and repolarizing ionic currents in rabbit ventricular cardiomyocytes under physiological self AP-clamp and sequential dissection of ionic currents using selective ion channel inhibitors (Table II in the [Data Supplement](#)). Each ionic current has its characteristic profile and magnitude during the AP shown in Figure 1. The rapid opening of voltage-gated Na^+ channels generates a transient Na^+ current, which is responsible for AP upstroke. The phase 1 repolarization of the AP is mediated by both the transient outward K^+ current and the Ca^{2+} -activated Cl^- current. During AP plateau phase, a small sustained I_{NaL} and a significantly larger but more rapidly inactivating L-type Ca^{2+} current are the predominant inward currents (Figure 1). Phase 3 repolarization is predominantly mediated by I_{Kr} , and then the inward rectifier K^+ current completes terminal repolarization (Figure 1). The slow delayed rectifier K^+ current and the Ca^{2+} -activated slow conductance K^+ current are small currents under a physiological ventricular AP in the absence of β -adrenergic stimulation. A significantly inward NCX ($\text{Na}^+/\text{Ca}^{2+}$ exchanger) current (Ca^{2+} removal) is present during (and even after) terminal repolarization. Importantly, relatively small ionic currents are flowing and balancing each other during the plateau phase of the AP. Two key ionic currents, I_{Kr} and I_{NaL} , achieve their peak density during the end of the plateau phase (Figure 1), suggesting that these currents may significantly influence APD and repolarization stability. Therefore, we focused on the mechanistic investigation of the relationship between I_{Kr} and I_{NaL} during normal and impaired repolarization.

Profile of I_{Kr} and I_{NaL} During Control, Shortened, and Prolonged APD

We recorded I_{Kr} and I_{NaL} during the cell's own AP shown in Figure 2 using self AP-clamp with physiological solutions, at 36°C and 2 Hz steady-state pacing frequency. In control, I_{Kr} is rapidly activated during the phase 3 repolarization of the AP, achieving a peak density of 0.84 ± 0.05 pA/pF (Figure 2A). In contrast, a persistent

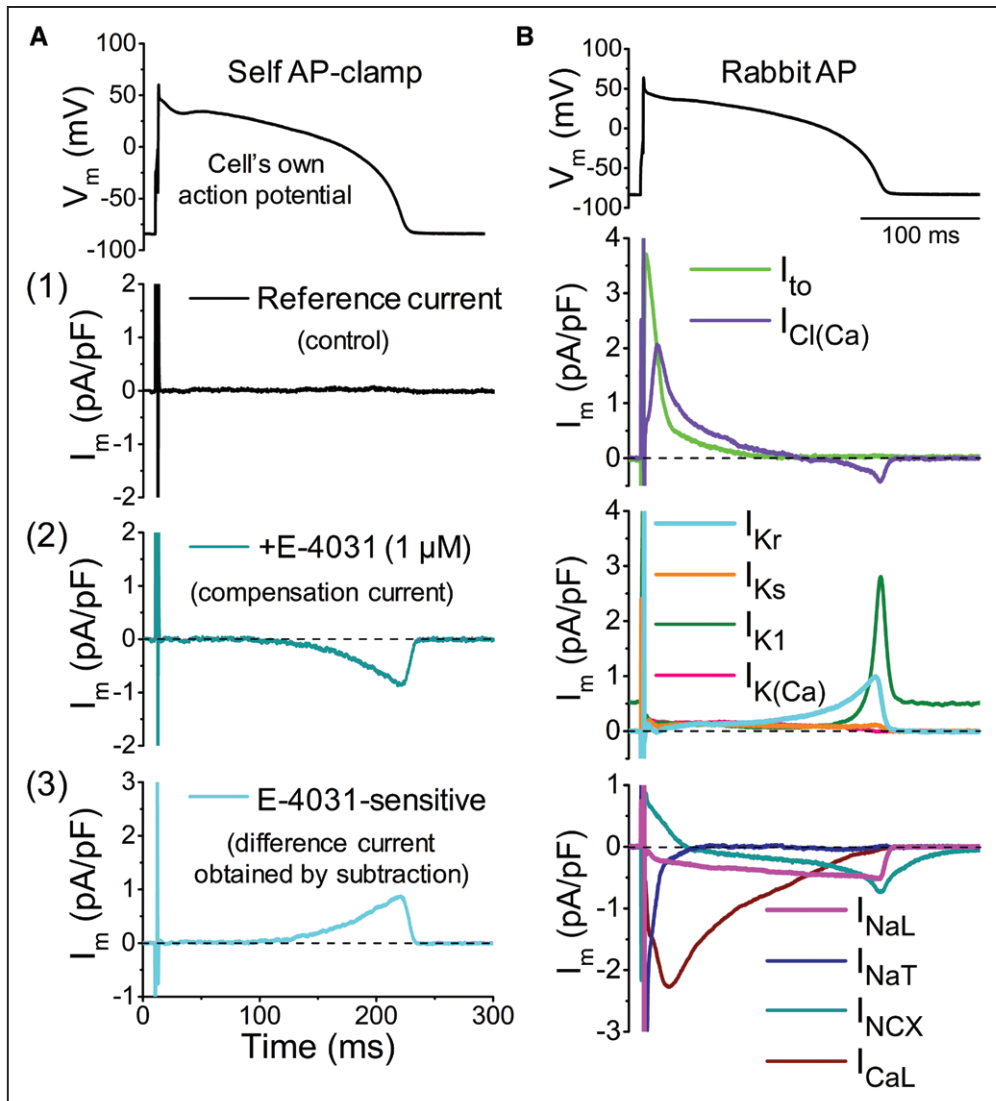


Figure 1. Profile of the major ionic currents in rabbit ventricular cardiomyocytes under physiological action potential (AP)-clamp.

A, Self AP-clamp technique to measure ionic currents under physiological AP. First, recording the cell's own steady-state AP, then using this AP as voltage command a predrug control or reference current (1) is obtained. Next, when a drug is applied (eg, E-4031), a compensation current (2) is recorded specific to the drug action. The drug-sensitive current (3) is obtained as the difference current (ie, subtracting the compensation current from the reference current). **B**, Representative traces of major ionic currents in rabbit ventricular cardiomyocytes under physiological AP-clamp. Ionic currents were measured as drug-sensitive currents. Cells were paced at 2 Hz steady-state frequency at 36°C. Transient outward K^+ current (I_{to}) and calcium-activated Cl^- current ($I_{Cl(Ca)}$) were measured as 4-aminopyridine and CaCCinh-A01-sensitive currents, respectively. Rapid delayed rectifier K^+ current (I_{Kr}), slow delayed rectifier K^+ current (I_{Ks}), inward rectifier K^+ current (I_{K1}), and small conductance Ca^{2+} -activated K^+ current ($I_{K(Ca)}$) were measured as E-4031, HMR-1556, Ba^{2+} , and apamin-sensitive currents, respectively. Late Na^+ current (I_{NaL}), transient Na^+ current (I_{NaT}), Na^+/Ca^{2+} exchange current (I_{NCX}), and L-type Ca^{2+} current (I_{CaL}) were measured as GS-967, tetrodotoxin, ORM-10962, and nifedipine-sensitive currents, respectively. The peak of I_{NaT} is out of range.

I_{NaL} was present throughout the entire AP plateau; however, I_{NaL} achieved a peak density of -0.55 ± 0.03 pA/pF (35% less than I_{Kr} magnitude, $P < 0.001$) also at the phase 3 of the AP when the driving force for Na^+ entry is increased. Although I_{NaL} rises earlier than I_{Kr} during the AP plateau (Figure 2A), the net charge carried by I_{NaL} versus I_{Kr} during the AP was similar (Figure 2E and 2F inset; 0.056 ± 0.004 versus 0.063 ± 0.004 pC/pF, respectively; $P = 0.17$). Even more striking is that the integrated I_{NaL} and I_{Kr} fluxes covary in individual cells, independent of

APD (Figure 2I and 2J), which raises the possibility that channel expression might covary (see below).

In another set of experiments, cell pretreatment with I_{Kr} inhibitor E-4031 (1 μ mol/L) prolonged APD (pharmacologically induced LQT2 model). Self AP-clamp using prolonged APD (Figure 2B) led to increased I_{NaL} peak density (by 26%) and net charge (by 88%) versus control (Figure 2E and 2F). Next, pretreatment of the cell with the I_{NaL} inhibitor GS-967 (1 μ mol/L) shortened APD (pharmacologically induced SQT model). Self AP-clamp using shortened APD (Figure 2C) led to reduced

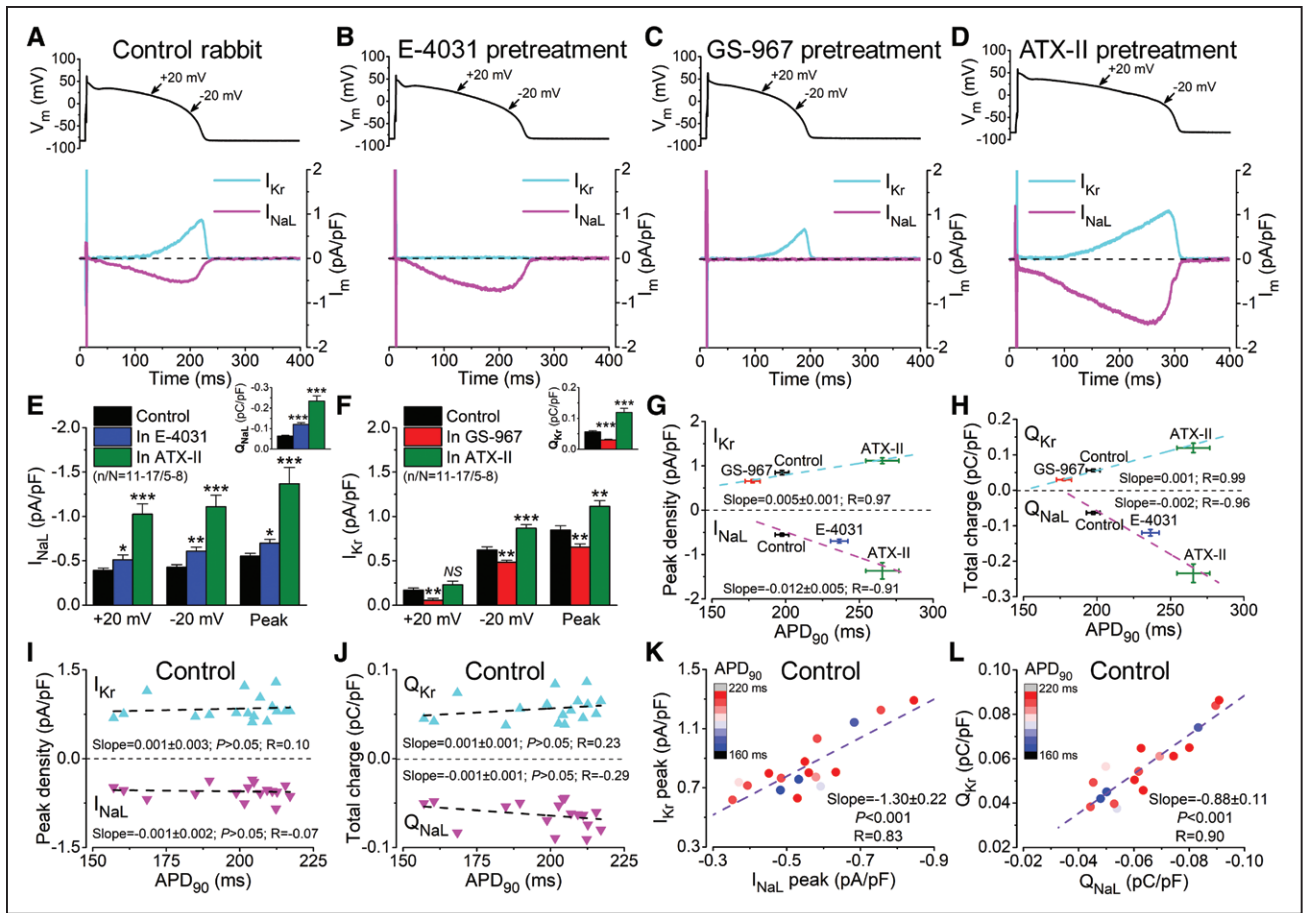


Figure 2. Correlation between rapid delayed rectifier K^+ current (I_{Kr}) and late Na^+ current (I_{NaL}) under self action potential (AP)-clamp.

A, I_{Kr} and I_{NaL} under self AP-clamp in control rabbit ventricular cardiomyocytes. I_{NaL} and I_{Kr} were measured as 1 μ mol/L GS-967 and 1 μ mol/L E-4031-sensitive currents, respectively. Cells were paced at 2 Hz. **B**, I_{NaL} under a prolonged AP duration (APD) following I_{Kr} inhibition (E-4031 pretreatment). **C**, I_{Kr} under a shortened APD following I_{NaL} inhibition (GS-967 pretreatment). **D**, I_{NaL} and I_{Kr} under a prolonged APD following sea anemone toxin II (ATX-II; 5 nmol/L) treatment to modulate Na^+ channel inactivation. **E** and **F**, I_{Kr} and I_{NaL} densities in control, and following pretreatment with either E-4031, GS-967, or ATX-II. Inset shows the net charge carried by I_{NaL} and I_{Kr} under self AP-clamp. **G** and **H**, Correlation between APD and I_{Kr} or I_{NaL} peak densities and net charges measured in control and following pretreatment with either E-4031, GS-967, or ATX-II. **I** and **J**, No correlation between APD and I_{Kr} or I_{NaL} peak densities and net charges in individual control cells under self AP-clamp. **K** and **L**, Correlation between I_{Kr} and I_{NaL} peak densities and net charges obtained in each control cell under self AP-clamp. Dashed lines represent the fitted linear regression curves. Mean \pm SEM is shown. n/N refers to cells/animals measured in each group. ANOVA with Bonferroni post test. NS indicates not significant ($P>0.05$). * $P<0.05$, ** $P<0.01$, *** $P<0.001$.

I_{Kr} peak density (by 23%) and net charge (by 47%) versus control (Figure 2E and 2F). Sea anemone toxin II (ATX-II, 5 nmol/L) that impairs Na^+ channel inactivation prolonged APD (pharmacologically induced LQT3 model) and markedly increased I_{NaL} under self AP-clamp (Figure 2D). ATX-II increased I_{NaL} peak density by 148% and net charge by 268% versus control; however, the prolonged APD by ATX-II also led to increased I_{Kr} peak density by 32% and net charge by 113% versus control (Figure 2E and 2F). These acute manipulations of I_{Kr} and I_{NaL} and APD exemplify that in addition to the covarying I_{Kr} and I_{NaL} at baseline, the acute changes in APD evoke inherent biophysical coordination between I_{Kr} and I_{NaL} (Figure 2G and 2H). That is, if APD is prolonged by excess I_{NaL} , the long APD promotes more I_{Kr} to limit APD prolongation.

Further analyzing the relationship between I_{Kr} and I_{NaL} , there was a >2-fold variation in both I_{Kr} and I_{NaL} magnitudes under self AP-clamp already in control cells (Figure 2I and 2J). Peak current densities in control varied in individual myocytes between 0.62 to 1.29 pA/pF and 0.35 to 0.84 pA/pF for I_{Kr} and I_{NaL} , respectively (Figure 2I). However, there was no correlation in control between the cells' baseline APD_{90} and either I_{Kr} and I_{NaL} peak densities (Figure 2I) or total charges (Figure 2J) under self AP-clamp. Despite the large cell-to-cell variability, I_{Kr} and I_{NaL} magnitudes were not randomly distributed, but instead, I_{Kr} and I_{NaL} peak densities and net charges were highly correlated when measured in the same cell under self AP-clamp (Figure 2K and 2L). It also showed that similar APD_{90} (or APD_{25} or APD_{50} , Figure I in the Data Supplement) can be generated by

largely different, but matched, I_{Kr} and I_{NaL} densities and net charges. These data suggest that I_{Kr} and I_{NaL} might be coregulated not only biophysically but also in their functional expression.

Altered I_{NaL}/I_{Kr} Balance in HF

HF is known to be associated with arrhythmogenic electrophysiological remodeling, including changes in I_{NaL} and I_{Kr} that leads to APD prolongation.^{18,22} We measured the

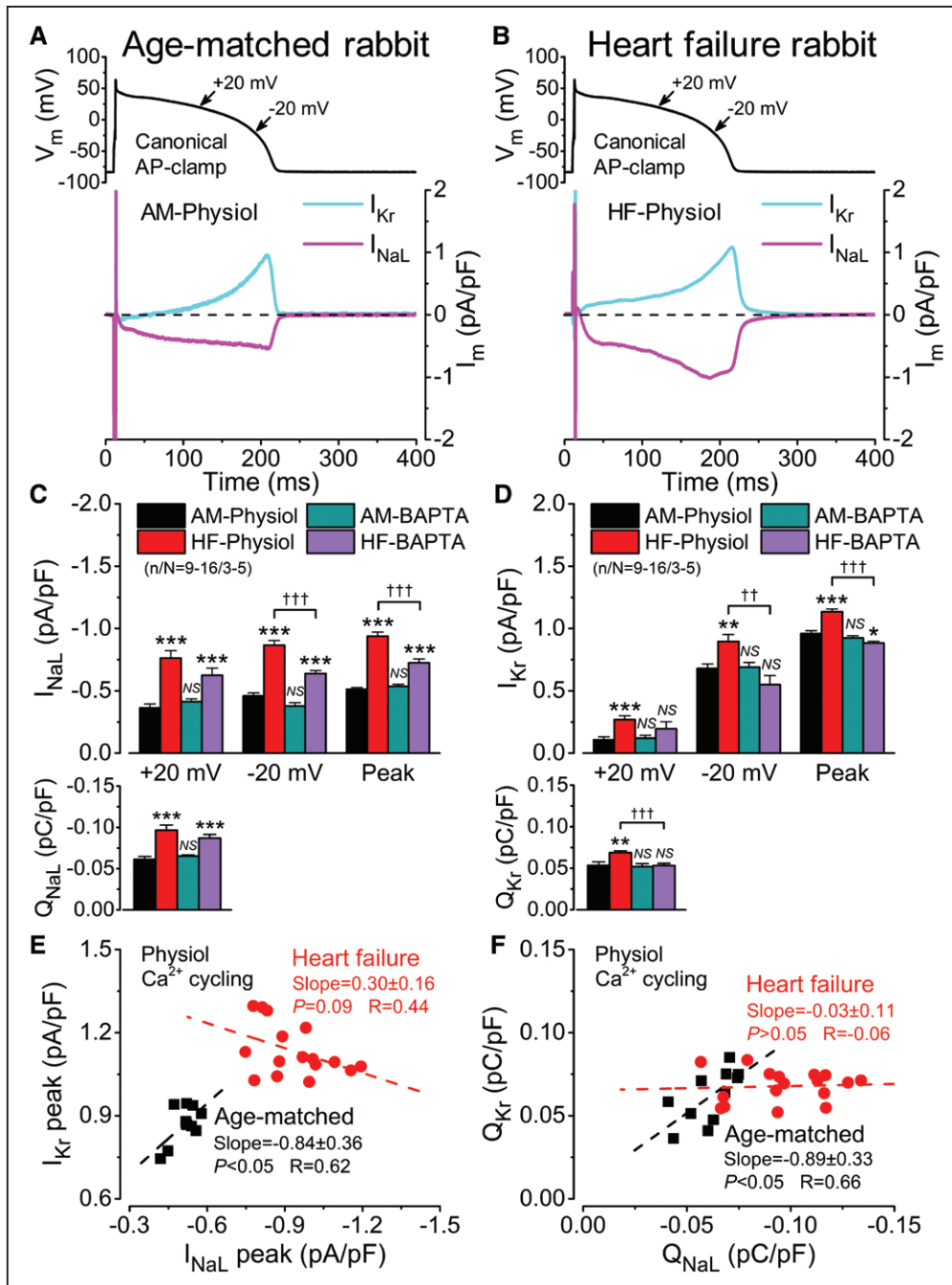


Figure 3. Heart failure shifts the balance between rapid delayed rectifier K⁺ current (I_{Kr}) and late Na⁺ current (I_{NaL}) in rabbit ventricular cardiomyocytes.

A and **B**, I_{Kr} and I_{NaL} in rabbit heart failure (HF) and age-matched control (AM) under canonical action potential (AP)-clamp. I_{NaL} and I_{Kr} were measured as 1 μ M/L GS-967 and 1 μ M/L E-4031-sensitive currents under AP-clamp, respectively. Cells were paced at 2 Hz using the same, prerecorded AP. **C** and **D**, I_{NaL} and I_{Kr} densities and net charges in HF and AM measured under physiological AP-clamp with preserved Ca²⁺ transient (Physiol) or in the presence of 10 mmol/L BAPTA in the pipette to eliminate Ca²⁺ transient (BAPTA). **E** and **F**, Correlation between I_{Kr} and I_{NaL} peak densities and net charges in HF and AM. Dashed lines represent the fitted linear regression curves. Mean \pm SEM is shown. n/N refers to cells/animals measured in each group. ANOVA with Bonferroni post test. NS indicates not significant ($P > 0.05$). * $P < 0.05$, ** $P < 0.01$, *** $P < 0.001$ vs AM-Physiol; †† $P < 0.01$, ††† $P < 0.001$ vs HF-Physiol.

profiles of I_{Kr} and I_{NaL} in HF versus AM under the same, prerecorded, typical rabbit AP (canonical AP-clamp; Figure 3). I_{NaL} peak density was markedly increased in HF versus AM (-0.94 ± 0.03 versus -0.51 ± 0.01 pA/pF, $P < 0.001$), whereas I_{Kr} peak density was slightly increased in HF versus AM (1.13 ± 0.02 versus 0.96 ± 0.02 pA/pF, $P < 0.001$) under canonical AP-clamp shown in Figure 3A through 3D. This resulted in a 58% increase of I_{NaL} net charge in contrast to 29% increase of I_{Kr} net charge in HF versus AM (Figure 3C and 3D). Therefore, the balance between I_{NaL} and I_{Kr} is shifted toward enhanced depolarization in HF. Further analysis revealed that a significant correlation between I_{Kr} and I_{NaL} magnitudes in AM (ie, larger I_{Kr} in those cells having larger I_{NaL}) occurs not only in self AP-clamp (Figure 2K and 2L) but also under a canonical AP-clamp (Figure 3E and 3F). Importantly, this correlation was lost in HF, and rather an opposite tendency was found (ie, reduced I_{Kr} is concurrent with larger I_{NaL}) under AP-clamp (Figure 3E and 3F), which may reflect the altered regulation and remodeling of the channels in HF. HF is characterized by impaired intracellular Ca^{2+} handling and Ca^{2+} -dependent signaling including upregulation of CaMKII (Ca^{2+} /calmodulin-dependent protein kinase II).²⁵ Therefore, we repeated I_{NaL} and I_{Kr} measurements using 10 mmol/L BAPTA in the pipette to buffer $[Ca^{2+}]_i$ to nominally zero (Figure 1I in the Data Supplement). BAPTA significantly reduced I_{NaL} peak

density in HF (-0.72 ± 0.03 pA/pF, $P < 0.001$) but not in AM (Figure 3C). Moreover, BAPTA slightly reduced I_{Kr} in HF versus AM (0.88 ± 0.01 pA/pF, $P < 0.001$), whereas I_{Kr} was not changed by BAPTA in AM (Figure 3D).

I_{Kr} and I_{NaL} Counterbalance Under Control, Shortened, and Prolonged APD

We tested the impact of I_{Kr} and I_{NaL} inhibition on APD in control and disease models. The I_{Kr} inhibitor E-4031 (1 μ mol/L) significantly prolonged APD₉₀ in healthy rabbit ventricular cardiomyocytes (245.1 ± 5.8 versus 201.0 ± 5.1 ms, $P < 0.001$) shown in Figure 4A. E-4031 affected the phase 3 repolarization (Figure 4E) of the AP by increasing the plateau potential measured at 75% of APD₉₀ (Plateau₇₅) and decreasing the maximal rate of repolarization ($-dV/dt_{max}$). Application of the I_{NaL} inhibitor GS-967 (1 μ mol/L) in the E-4031 pretreated cells shortened APD₉₀ back to control (199.7 ± 6.6 ms, $P = 0.58$) by increasing $-dV/dt_{max}$ (Figure 4A and 4E). Next, reversing the order of the treatments, I_{NaL} inhibition using GS-967 significantly shortened APD₉₀ in control (177.3 ± 5.1 versus 206.9 ± 2.6 ms, $P < 0.001$) as shown in Figure 4B. GS-967 slightly depressed AP plateau potentials and accelerated phase 3 (Figure 4B and 4F). However, inhibiting I_{Kr} following GS-967 treatment restored

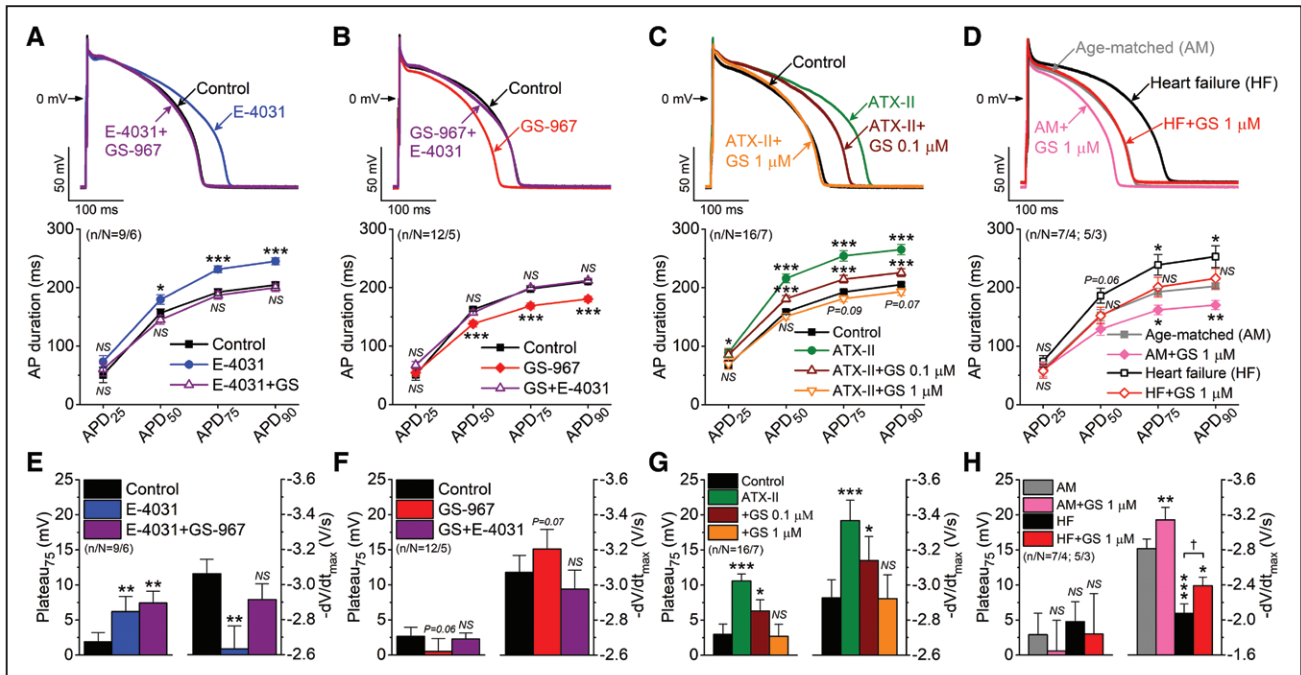


Figure 4. Rapid delayed rectifier K^+ current (I_{Kr}) and late Na^+ current (I_{NaL}) counterbalance each other on shaping the ventricular action potential (AP).

A, I_{NaL} inhibition (GS-967, 1 μ mol/L) abolished AP duration (APD) prolongation induced by I_{Kr} blockade (E-4031, 1 μ mol/L). **B**, I_{Kr} inhibition reverts AP shortening induced by I_{NaL} blockade. **C**, I_{NaL} inhibition abolished AP prolongation caused by modulated Na^+ channel inactivation using sea anemone toxin II (ATX-II, 5 nmol/L). **D**, I_{NaL} inhibition abolished AP prolongation in heart failure (HF). APDs at different phases of repolarization are shown below the representative AP traces. Cells were paced at 2 Hz. **E–H**, Plateau₇₅ potential and maximal rate of repolarization ($-dV/dt_{max}$). Mean \pm SEM is shown. n/N refers to cells/animals measured in each group. ANOVA with Bonferroni post test. AM indicates age-matched control; and NS, not significant ($P > 0.05$). * $P < 0.05$, ** $P < 0.01$, *** $P < 0.001$ vs control; † $P < 0.05$ vs HF.

APD₉₀ again to control (209.0±4.0 ms, $P=0.66$ versus control).

In another cellular model of long QT, ATX-II (5 nmol/L) treatment was used to enhance I_{NaL} and significantly prolong APD₉₀ (265.1±8.9 versus 201.5±3.2 ms, $P<0.001$) shown in Figure 4C. ATX-II increased Plateau₇₅ as expected, but interestingly, ATX-II also accelerated the rate of repolarization (Figure 4G) in line with I_{Kr} accumulation under the elevated AP plateau and prolonged APD. I_{NaL} inhibitor GS-967 at a concentration of 100 nmol/L significantly shortened APD₉₀ following ATX-II treatment (222.4±6.7 ms, $P<0.01$ versus ATX-II only), whereas a higher concentration of GS-967 (1 μmol/L) abolished the ATX-II-induced APD₉₀ prolongation (189.6±5.8 ms, $P=0.07$ versus control) and reduced Plateau₇₅ to control (Figure 4G). I_{NaL} was also enhanced in HF (Figure 3), and APD₉₀ was prolonged in HF versus AM (253.1±18.5 versus 202.4±5.8 ms, $P<0.05$) shown in Figure 4D. Importantly, the I_{NaL} inhibitor GS-967 (1 μmol/L) shortened APD₉₀ in HF back to control (215.9±16.6 ms, $P>0.05$ versus control) and increased $-dV/dt_{max}$ (Figure 4H).

Impact of I_{Kr} and I_{NaL} on Repolarization Stability

Next, we tested the contribution of I_{Kr} and I_{NaL} to the temporal dispersion of APD to assess repolarization stability.

I_{Kr} inhibition (E-4031, 1 μmol/L) significantly increased the STV of APD₉₀ (3.6±0.4 versus 2.5±0.1 ms, $P<0.001$), whereas I_{NaL} inhibition (GS-967, 1 μmol/L) significantly decreased STV (1.6±0.1 versus 2.6±0.2 ms, $P<0.001$) shown in Figure 5A and 5B in line with their effect on averaged APD₉₀ (Figure 4). However, combined I_{Kr} + I_{NaL} inhibition reduced STV below control (1.9±0.2 ms, $P<0.001$), despite the unchanged averaged APD₉₀. ATX-II robustly increased STV (5.0±0.6 versus 2.2±0.1 ms, $P<0.001$), shown in Figure 5C. Interestingly, partial blockade (0.1 μmol/L GS-967) of the enhanced I_{NaL} (by ATX-II) reduced STV to control (2.6±0.3 ms, $P>0.05$ versus control), whereas APD₉₀ was still significantly prolonged (compare Figures 5C and 4C). Moreover, higher concentration of GS-967 (1 μmol/L) decreased STV below control (1.7±0.2 ms, $P<0.05$ versus control) even in the presence of ATX-II (Figure 5C). STV was also markedly increased in HF versus AM (4.4±0.5 versus 2.6±0.3 ms, $P<0.05$), and importantly, I_{NaL} inhibition restored not only APD₉₀ but also STV to control (2.7±0.4 ms, $P>0.05$ versus AM) shown in Figure 5D.

To further analyze the beat-to-beat variability of APD₉₀, cumulative distribution of APD₉₀-variability in consecutive beats was calculated (Figure 5E through 5H). It showed that I_{Kr} inhibition (E-4031, 1 μmol/L) enhanced STV by markedly increasing the number of beats having large

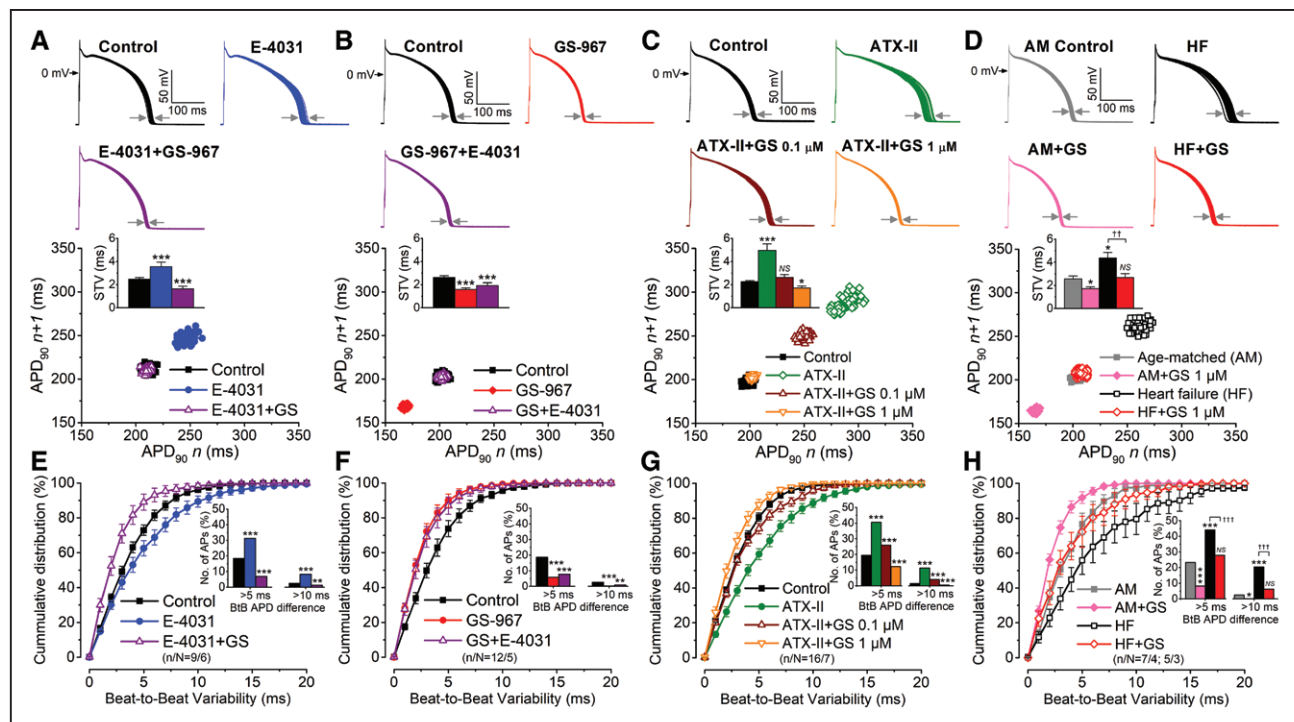


Figure 5. Impact of rapid delayed rectifier K⁺ current (I_{Kr}) and late Na⁺ current (I_{NaL}) on beat-to-beat (BtB) and short-term variabilities of action potential duration (APD).

A–D, Representative AP series and Poincare plots constructed using 50 consecutive APs at steady-state 2 Hz pacing. Inset shows the short-term variability (STV) of APD. **E–H**, Cumulative distribution curves of BtB changes in APD. I_{Kr} inhibition (E-4031, 1 μmol/L), I_{NaL} enhancement (sea anemone toxin II [ATX-II], 5 nmol/L), and heart failure (HF) increased APD-variability, whereas I_{NaL} inhibition (GS-967, 1 μmol/L) significantly reduced APD-variability. Insets show the number of APs having >5 and 10 ms BtB variability of APD. Mean±SEM is shown. n/N refers to cells/animals measured in each group. ANOVA with Bonferroni post test. AM indicates age-matched control; and NS, not significant ($P>0.05$). * $P<0.05$, ** $P<0.01$, *** $P<0.001$ vs control; †† $P<0.01$, ††† $P<0.001$ vs HF.

differences between consecutive APD_{90} values (>5 and >10 ms; shown as long tails in the distribution curve), but the median beat-to-beat variability was similar to control (Figure 5E). However, I_{NaL} inhibition decreased both the median beat-to-beat variability and markedly reduced the number of APs having large differences in APD_{90} values in consecutive beats (Figure 5F). In agreement with this role of I_{NaL} , ATX-II treatment significantly increased both the median and large APD_{90} beat-to-beat variabilities in consecutive beats, which were then reverted by GS-967

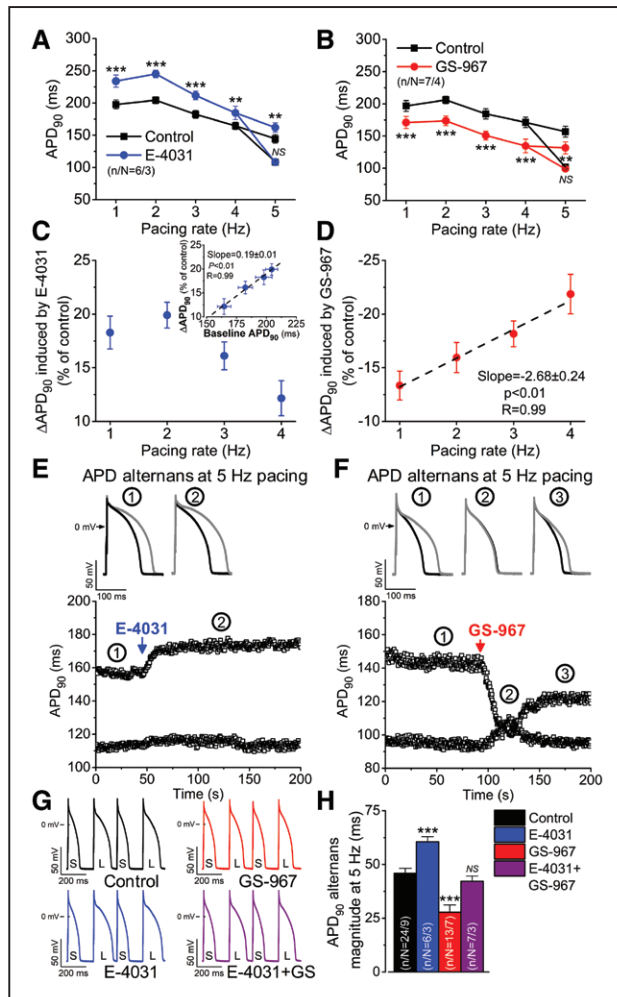


Figure 6. Frequency-dependent effect of rapid delayed rectifier K^+ current (I_{Kr}) and late Na^+ current (I_{NaL}) inhibition on action potential duration (APD).

A, Frequency-dependence of I_{Kr} inhibition. **B**, Frequency-dependence of I_{NaL} inhibition. **C**, Frequency-dependence of the E-4031-induced change in APD. Inset shows the correlation between the E-4031-induced change in APD and the baseline APD. **D**, Correlation between the pacing rate and GS-967-induced change in APD. Dashed line represents the fitted linear regression curve. **E** and **F**, Timing of E-4031 (1 μ mol/L) and GS-967 (1 μ mol/L) effects on APD alternans at 5 Hz steady-state pacing. Insets show representative APs at time points indicated. **G** and **H**, Representative AP series and APD alternans magnitudes. Mean \pm SEM is shown. n/N refers to cells/animals measured in each group. Paired Student *t* test. L indicates long APD; NS, not significant ($P>0.05$); and S, short APD. ** $P<0.01$, *** $P<0.001$.

(Figure 5G). Similarly, significantly enhanced beat-to-beat APD_{90} -variability was found in HF just as in ATX-II, and I_{NaL} inhibition significantly reduced beat-to-beat repolarization variability in HF (Figure 5H).

Frequency-Dependence of I_{Kr} and I_{NaL} Inhibition

We also examined the frequency-dependence of I_{Kr} and I_{NaL} inhibition. I_{Kr} inhibition (E-4031, 1 μ mol/L) caused a reverse-rate dependent lengthening of the APD_{90} (Figure 6A), and further analysis revealed that the observed APD_{90} prolongation was rather dependent on baseline APD_{90} (Figure 6C). Surprisingly, I_{NaL} inhibition (GS-967, 1 μ mol/L) induced more pronounced APD shortening at higher pacing rates (Figure 6B). This positive rate-dependence of GS-967 effect on APD_{90} (Figure 6D) is the opposite to that expected based on the reduced Na^+ channel availability, but the use-dependent drug-binding and the significant CaMKII-dependent modulation of I_{NaL} may be more important at rapid pacing rates.

In rabbit ventricular myocytes APD alternans occurred at high pacing rates (at 5 Hz at 36°C). The amplitude of the APD alternans was increased by I_{Kr} inhibition and decreased by I_{NaL} inhibition (Figure 6E and 6F). Interestingly, during APD alternans, only the long APD_{90} but not the short APD_{90} was altered by either E-4031 or GS-967. Moreover, GS-967 treatment transiently abolished APD alternans, then the magnitude of the APD alternans (the difference between long and short APDs) achieved a steady-state (in 60–90 seconds) at a reduced level compared with control (Figure 6F). This observation may reflect changes in $[Na^+]_i$ and $[Ca^{2+}]_i$, which require further investigation. Importantly, combined application of E-4031 and GS-967 restored the magnitude of APD alternans at 5 Hz to control (Figure 6G and 6H), suggesting a counterbalance between I_{Kr} and I_{NaL} also at high pacing rates.

Relationship Between I_{Kr} and I_{NaL} in Control and Ischemic HF Pigs

Next, we tested whether the correlation between I_{Kr} and I_{NaL} is present in another large animal model relevant to human electrophysiology. I_{NaL} measured under physiological self AP-clamp in control porcine ventricular myocytes was smaller (-0.33 ± 0.01 pA/pF), whereas I_{Kr} density was slightly larger (0.99 ± 0.04 pA/pF) than those measured in rabbit (compare Figure 7 and Figure 2). However, I_{NaL} total charge (0.050 ± 0.004 pC/pF) was still similar to that measured in rabbits because of the longer APD_{90} (227.9 ± 17.7 ms) in pigs (Figure 7C). Importantly, we found statistically significant correlation between both peak densities and total charges of I_{NaL} and I_{Kr} under self AP-clamp also in pigs (Figure 7E and 7F).

Chronic ischemic HF (5 months postmyocardial infarction) in pigs led to APD_{90} prolongation (246.1 ± 12.9 ms)

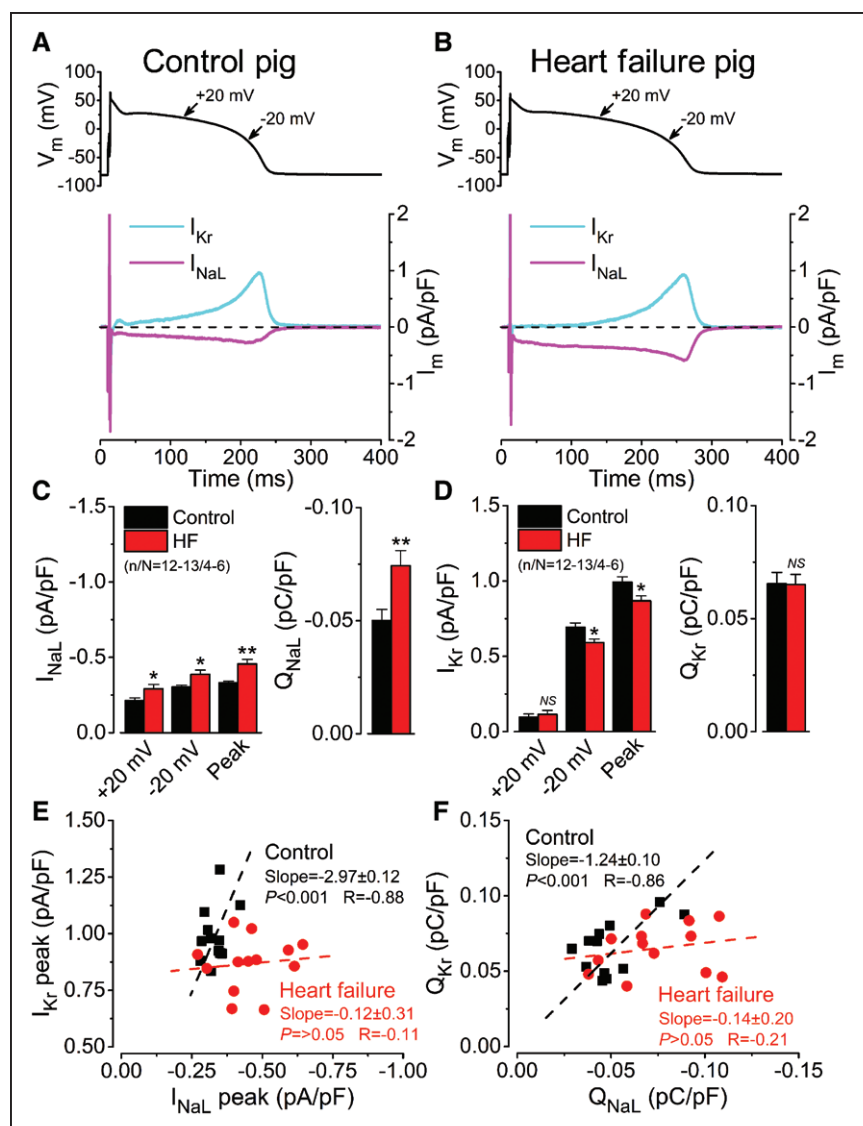


Figure 7. Rapid delayed rectifier K^+ current (I_{Kr}) and late Na^+ current (I_{NaL}) in control and ischemic heart failure (HF) porcine ventricular myocytes under self action potential (AP)-clamp.

A and B, I_{Kr} and I_{NaL} in porcine ventricular cardiomyocytes under self AP-clamp in control and ischemic HF induced by chronic myocardial infarction (5-month postmyocardial infarction). I_{NaL} and I_{Kr} were measured as 1 μ mol/L GS-967 and 1 μ mol/L E-4031-sensitive currents under self AP-clamp, respectively. Cells were paced at 1 Hz. **C and D,** I_{NaL} and I_{Kr} densities and net charges in control and HF. **E and F,** Correlation between I_{Kr} and I_{NaL} peak densities and net charges under self AP-clamp. Dashed lines represent the fitted linear regression curves. Mean \pm SEM is shown. n/N refers to cells/animals measured in each group. ANOVA with Bonferroni post test. NS indicates not significant ($P > 0.05$). * $P < 0.05$, ** $P < 0.01$.

and remodeling in both I_{NaL} and I_{Kr} in myocytes isolated from the remote zone of the infarct (Figure 7B). However, I_{NaL} was only slightly increased (by 38%) in porcine ischemic HF (Figure 7C), whereas I_{NaL} was markedly increased (by 84%) in nonischemic (volume/pressure-overload) rabbit HF (Figure 3C). At the same time, I_{Kr} decreased by 13% in porcine ischemic HF (Figure 7D) as opposed to 18% increase in nonischemic rabbit HF (Figure 3D). These results suggest a differential remodeling between ischemic versus nonischemic HF in the 2 species. However, the significant correlation between I_{Kr} and I_{NaL} was absent in both HF models.

DISCUSSION

Contribution of I_{Kr} and I_{NaL} to AP Morphology

Imbalance between depolarizing and repolarizing currents results in abnormal AP morphology and APD changes in cardiac myocytes that manifest as altered QT interval on

the ECG. Our data demonstrate that I_{Kr} and I_{NaL} are not only major determinants of APD, but they counterbalance each other during the physiological AP of rabbit ventricular cardiomyocytes (Figures 2 and 4). Importantly, I_{Kr} and I_{NaL} peak densities and peak charges measured in the same cell significantly correlated with each other (but not with the baseline APD) both in rabbit (Figure 2) and porcine cardiomyocytes (Figure 7), despite >2-fold cell-to-cell variability in their magnitudes in control. Moreover, the significant statistical correlation between I_{Kr} and I_{NaL} was still present using a canonical AP-clamp (ie, same voltage profile; Figure 3) in line with the recently demonstrated coupled transcription and functional expression of $Na_v1.5$ and hERG.²⁶ Furthermore, if one of these currents is either reduced or enhanced leading to impaired AP repolarization, compensatory changes in the other current—dictated by the altered APD and plateau voltages—will affect the outcome on APD₉₀ and repolarization stability (Figure 2). The counterbalance between I_{Kr} and I_{NaL} on AP repolarization may have significant clinical

implications, and the I_{Kr}/I_{NaL} balance may represent an important antiarrhythmic target.

I_{Kr} is considered a major repolarizing current affecting APD and repolarization stability²⁷ in ventricular cardiomyocytes of larger mammals, including humans.² However, the strong statistical correlation between the net charges of I_{Kr} and I_{NaL} (in rabbits, Figure 2L; in pigs, Figure 7F), as well as the opposing impact of these currents on APD (Figure 4) and repolarization stability (Figure 5) are striking yet not completely unexpected findings, as previously reviewed.⁹ Most previous studies measured a smaller I_{NaL} of ≈ -0.3 pA/pF at -20 mV in both human,²⁸ canine,²⁹ and rabbit³⁰ ventricular myocytes under conventional square voltage pulses and in the presence of strong intracellular Ca^{2+} buffers to eliminate $[Ca^{2+}]_i$ transient. However, CaMKII has been previously demonstrated to significantly upregulate I_{NaL} .^{29,31,32} This physiological CaMKII-dependent upregulation of I_{NaL} might have been missed in earlier biophysical studies, but our more physiological conditions to measure I_{NaL} (with preserved Ca^{2+} transient and CaMKII activation under the AP) was able to reveal the true magnitude of the current.^{5,33} We found a smaller I_{NaL} peak density under self AP-clamp in porcine ventricular myocytes (Figure 7) than in rabbit; however, I_{NaL} net charge was similar to that in rabbit because of the longer APD in pigs. Previous studies used tetrodotoxin almost exclusively to measure I_{NaL} raising a dilemma. Cardiac Na^+ channels (predominantly $Na_v1.5$) are insensitive to tetrodotoxin with an IC_{50} of 1 to 2 $\mu\text{mol/L}$.^{34,35} Thus, higher concentrations of tetrodotoxin (10 to 30 $\mu\text{mol/L}$) are needed to achieve complete Na^+ channel inhibition in cardiomyocytes, which may have off-target effect on L-type Ca^{2+} channels.³⁶ The other option is to use lower concentrations of tetrodotoxin, but in this case, the magnitude of I_{NaL} will be underestimated. Hence, we used GS-967 which does not have such off-target effect and exhibits higher selectivity for I_{NaL} over transient Na^+ current.^{30,33}

The positive rate-dependence of GS-967 effect on APD_{90} (Figure 6) is a conflicting finding with previous reports showing smaller I_{NaL} at higher frequency stimulation.¹¹ Possible explanations may include the state-dependent binding of GS-967 to the Na^+ channels³⁷ and significant CaMKII-dependent modulation of I_{NaL} at rapid pacing rates.³³ Interestingly, ranolazine also caused more pronounced QT shortening at rapid heart rates than during bradycardia in patients with LQT3.¹⁴ The underlying mechanisms require further investigation. On the contrary, I_{Kr} inhibition showed a well-known reverse-rate dependent effect on APD_{90} as it followed the frequency-dependent changes in baseline APD_{90} (Figure 6), which is characteristic to the myocardium.³⁸

Our AP-clamp data revealed that I_{NaL} activates earlier than I_{Kr} during the AP (Figure 2); thus, a significant I_{NaL} can be measured already under the mid-plateau phase of the AP where small depolarizing and repolarizing

currents delicately balance each other.⁶ This feature can be accountable for the strong influence of I_{NaL} inhibition on APD_{90} and repolarization stability, despite the small I_{NaL} amplitude in accordance with modeling data.^{7,8} Moreover, I_{NaL} inhibition may also decrease intracellular Na^+ and Ca^{2+} load that has been shown to occur under a prolonged APD,³⁹ during tachypacing-induced APD alternans⁴⁰ and in HF.⁴¹

Remodeling of I_{Kr} and I_{NaL} is frequently reported in HF,^{18,22,42} which introduces a shift in I_{Kr}/I_{NaL} balance and significantly contributes to the increased arrhythmia risk. We found enhanced I_{NaL} in both rabbit nonischemic HF (Figure 3) and porcine ischemic HF (Figure 7); however, I_{NaL} upregulation was more pronounced in the nonischemic model. I_{Kr} was slightly altered in HF in line with previous studies.⁴² I_{Kr} was downregulated in porcine ischemic HF (Figure 7), whereas a Ca^{2+} -dependent I_{Kr} upregulation was found in rabbit nonischemic HF (Figure 3). The mechanism of differential ion channel remodeling in ischemic versus nonischemic HF has not been elucidated yet.

Clinical and Preclinical Findings Supporting the Importance of I_{Kr}/I_{NaL} Balance

Targeting the balance between I_{Kr} and I_{NaL} may have significant therapeutic potential in QT abnormalities caused by either genetic or acquired conditions affecting these ion channels. Accordingly, mexiletine treatment was found to be effective in reducing the dispersion of repolarization and preventing torsades de pointes ventricular tachycardia in both LQT2 and LQT3 models.¹² Similarly, I_{Kr} inhibition in short QT syndrome represents a potential therapeutic approach to normalize the duration of repolarization; however, the mutant channels may express differential sensitivity for inhibitors.⁴³ Importantly, several antiarrhythmic drugs successfully used in clinic including amiodarone,⁴⁴ ranolazine,⁴⁵ flecainide, and quinidine⁴⁶ inhibit both I_{Kr} and I_{NaL} . These drugs, previously thought to have off-target effects, may finetune the ratio between I_{Kr}/I_{NaL} block to exert antiarrhythmic effects. Understanding the importance of the counterbalancing effect of I_{Kr} and I_{NaL} , the ratio between I_{Kr}/I_{NaL} block needs to be considered when choosing an appropriate drug to treat a specific clinical condition.

Our experimental results confirm the predictions of a quantitative computational model⁴⁷ showing that selective I_{NaL} inhibition has beneficial effects on several factors considered to be proarrhythmic in LQT as I_{NaL} inhibition suppressed APD prolongation (Figure 4), beat-to-beat repolarization instability (Figure 5) and APD alternans (Figure 6). These results are in accordance with the effective suppression of reentrant and multifocal ventricular fibrillation by I_{NaL} inhibition.⁴⁸

When the repolarization is compromised, it may impair $[Na^+]_i$ and $[Ca^{2+}]_i$ homeostasis leading to CaMKII activation and generation of reactive oxygen species, which then feedback on ion channels forming a vicious cycle.^{49,50} It is particularly true for HF, which is characterized by reduced repolarization reserve, increased I_{NaL} , and enhanced CaMKII-mediated SR Ca^{2+} leak, all of them significantly increase the risk of arrhythmias.^{18,21,22,25} Therefore, breaking the detrimental positive feedback loop can have a large benefit, especially in HF, but also in LQT. Accordingly, inhibitors of CaMKII and I_{NaL} were found advantageous in numerous preclinical studies, but the confirmation of this concept in clinical trials is still yet to come.^{10,50}

Clinical and Preclinical Findings Limiting the Importance of I_{Kr}/I_{NaL} Balance

Despite the strong coupling between I_{Kr} and I_{NaL} under physiological AP repolarization, we found the timing of these ionic currents during AP shows major differences. Our AP-clamp data indicate that I_{NaL} has more influence on mid-plateau potentials, and I_{Kr} predominantly affects phase 3 repolarization rate (Figures 2 and 4). These differences may explain (1) the differential susceptibility to EAD formation in LQT2 and LQT3 models^{51,52} and (2) the large differences in the clinical manifestations of LQT2 and LQT3.^{1,2} Moreover, the magnitude of both I_{Kr} and I_{NaL} significantly varies across species and exhibits significant spatial difference between cardiac regions.^{10,53}

I_{Kr}/I_{NaL} balance may also vary at different heart rates. I_{Kr} has activation and deactivation time constants of ≈ 100 to 200 ms and more rapid kinetics of inactivation and recovery from inactivation in rabbit and human ventricular cardiomyocytes; thus, I_{Kr} may accumulate at rapid heart rates.⁵³ I_{NaL} inactivation time constant is ≈ 600 ms, and I_{NaL} was reported to decrease with shorter diastolic intervals.¹¹ Patients with LQT2 and LQT3 (but not LQT1) have generally higher risk of arrhythmias at slower heart rates; however, in carriers of specific mutations (eg, S1904L in SCN5A encoding $Na_v1.5$), arrhythmia is more frequent at rapid heart rates.² Moreover, I_{NaL} was shown to be involved in reverse-rate dependence of I_{Kr} inhibition on APD¹¹ that can be proarrhythmic in patients treated with I_{Kr} inhibiting drugs or carrying LQT2 mutations.

Nonetheless, cardiac arrhythmias are frequently triggered by increased sympathetic activity in patients with LQT,^{1,2} which may shift the balance between inward and outward ionic currents including not only L-type Ca^{2+} current and slow delayed rectifier K^+ current^{54,55} but also I_{NaL} and I_{Kr} .⁵⁶ β -adrenergic agonist isoproterenol significantly enhances I_{NaL} via both protein kinase A and CaMKII-dependent mechanisms.³³ On the contrary I_{Kr} response to isoproterenol is variable between preparations and may involve regulation via protein kinase A and protein kinase C.¹⁸ Although similar EC_{50} values of isoproterenol (≈ 10

nmol/L) was found to activate I_{NaL} and I_{Kr} , the maximal responses were largely different (2.4- versus 1.1–1.3-fold increases for I_{NaL} and I_{Kr} , respectively),^{18,22,57} indicating that I_{Kr}/I_{NaL} balance is shifted during β -adrenergic stimulation. This may partially explain why β blockers are still the preferred treatment in patients with LQT as they significantly reduce the risk of arrhythmias.²

Perspectives

It has been previously shown that $Na_v1.5$ and $K_{ir2.1}$ exhibit coordinated expression and they traffic together from trans-Golgi to sarcolemma to control excitability,⁵⁸ whereas such coordination between $Na_v1.5$ and hERG may control repolarization stability in the heart, suggested recently by the coupled transcription and correlation of $Na_v1.5$ and hERG surface expression levels.²⁶ The quantitative correlation we see between mean I_{Kr} and I_{NaL} during the AP could reflect this type of transcriptional coregulation but may be, in part, a manifestation of inherent voltage-dependent feedback between the channels during AP plateau voltages. However, the remarkable $I_{NaL}-I_{Kr}$ correlation within individual cells (where cells with the same APD can have in parallel much higher I_{NaL} and I_{Kr}) makes the transcriptional coregulation an attractive hypothesis for future work. Future studies are needed to reveal the exact contribution of I_{NaL} and I_{Kr} to Na^+ and Ca^{2+} homeostasis under pathological conditions affecting AP repolarization because Ca^{2+} handling abnormalities further increase repolarization instability^{59,60} and trigger arrhythmias in the intact heart.⁶¹ Patient-specific human-induced pluripotent stem cell-derived cardiomyocytes can also provide important information on the different LQT phenotypes and their pharmacological modulation.⁶² Further in vivo arrhythmia tests in large animal LQT, SQT, and HF models, which exhibit human-like repolarization reserve⁶³ are necessary to assess the therapeutic potential of targeting the I_{Kr}/I_{NaL} balance.

ARTICLE INFORMATION

Received September 6, 2019; accepted March 16, 2020.

Affiliations

Department of Pharmacology (B.H., Y.C.-I., L.T.I., D.M.B., T.B.), Department of Biomedical Engineering (Y.C.-I.), and Department of Internal Medicine/Cardiology (Y.C.-I.), University of California, Davis. Amgen, Inc, South San Francisco (S.R.). InCarda Therapeutics, Inc, Newark, CA (L.B.); Department of Physiology, Faculty of Medicine, University of Debrecen, Hungary (T.B.).

Acknowledgments

We thank Zhong Jian, Rafael Shimkunas, Mark Jaradeh, Logan R.J. Bailey, Johanna M. Borst, Benjamin W. Van, Maura Ferrero, and Julie Bossutt for their help in animal care, cell isolation, and laboratory tasks. We thank William T. Ferrier, Linda Talken, Lynette M. Mendoza, and Kenneth S. Ginsburg for their help in surgical procedures and echocardiographic follow-up of heart failure rabbits. We also thank Leigh G. Griffiths, Kristin N. Grimsrud, Claus S. Sondergaard, and W. Douglas Boyd for their help in surgical procedures and echocardiographic follow-up of heart failure pigs.

Sources of Funding

This work was supported by grants from the National Institute of Health R01-HL090880 (Drs Izu and Chen-Izu), R01-HL123526 (Dr Chen-Izu), R01-

HL141460 (Dr Chen-lzu), P01-HL141084 (Dr Bers), R01-HL030077 (Dr Bers), and R01-HL142282 (DMB); the American Heart Association 14GRNT20510041 (Dr Chen-lzu); and the Hungarian Scientific Research Fund OTKA101196 (Dr Bányász).

Disclosures

Drs Belardinelli and Rajamani are former employees of Gilead Sciences, Inc (Foster City, CA), which is the patent holder of GS-967. The other authors report no conflicts.

REFERENCES

- Morita H, Wu J, Zipes DP. The QT syndromes: long and short. *Lancet* 2008;372:750–763. doi: 10.1016/S0140-6736(08)61307-0
- Bohnen MS, Peng G, Robey SH, Terrenoire C, Iyer V, Sampson KJ, Kass RS. Molecular pathophysiology of congenital long QT syndrome. *Physiol Rev* 2017;97:89–134. doi: 10.1152/physrev.00008.2016
- Antzelevitch C, Brugada P, Borggrefe M, Brugada J, Brugada R, Corrado D, Gussak I, LeMarec H, Nademanee K, Perez Riera AR, et al. Brugada syndrome: report of the second consensus conference: endorsed by the Heart Rhythm Society and the European Heart Rhythm Association. *Circulation* 2005;111:659–670. doi: 10.1161/01.CIR.0000152479.54298.51
- Brugada R, Hong K, Dumaine R, Cordeiro J, Gaita F, Borggrefe M, Menendez TM, Brugada J, Pollevick GD, Wolpert C, et al. Sudden death associated with short-QT syndrome linked to mutations in HERG. *Circulation* 2004;109:30–35. doi: 10.1161/01.CIR.0000109482.92774.3A
- Horvath B, Banyasz T, Jian Z, Hegyi B, Kistamas K, Nanasi PP, Izu LT, Chen-lzu Y. Dynamics of the late Na(+) current during cardiac action potential and its contribution to afterdepolarizations. *J Mol Cell Cardiol* 2013;64:59–68. doi: 10.1016/j.jmcc.2013.08.010
- Hegyí B, Bossuyt J, Griffiths LG, Shimkunas R, Coulibaly Z, Jian Z, Grimsrud KN, Sondergaard CS, Ginsburg KS, Chiamvimonvat N, et al. Complex electrophysiological remodeling in postinfarction ischemic heart failure. *Proc Natl Acad Sci U S A* 2018;115:E3036–E3044. doi: 10.1073/pnas.1718211115
- Noble D, Noble PJ. Late sodium current in the pathophysiology of cardiovascular disease: consequences of sodium-calcium overload. *Heart* 2006;92(suppl 4):iv1–iv5. doi: 10.1136/hrt.2005.078782
- Yang PC, Song Y, Giles WR, Horvath B, Chen-lzu Y, Belardinelli L, Rajamani S, Clancy CE. A computational modelling approach combined with cellular electrophysiology data provides insights into the therapeutic benefit of targeting the late Na+ current. *J Physiol* 2015;593:1429–1442. doi: 10.1113/jphysiol.2014.279554
- Zaza A, Rocchetti M. The late Na+ current—origin and pathophysiological relevance. *Cardiovasc Drugs Ther* 2013;27:61–68. doi: 10.1007/s10557-012-6430-0
- Belardinelli L, Giles WR, Rajamani S, Karagueuzian HS, Shryock JC. Cardiac late Na+ current: proarrhythmic effects, roles in long QT syndromes, and pathological relationship to CaMKII and oxidative stress. *Heart Rhythm* 2015;12:440–448. doi: 10.1016/j.hrthm.2014.11.009
- Wu L, Ma J, Li H, Wang C, Grandi E, Zhang P, Luo A, Bers DM, Shryock JC, Belardinelli L. Late sodium current contributes to the reverse rate-dependent effect of IKr inhibition on ventricular repolarization. *Circulation* 2011;123:1713–1720. doi: 10.1161/CIRCULATIONAHA.110.000661
- Shimizu W, Antzelevitch C. Sodium channel block with mexiletine is effective in reducing dispersion of repolarization and preventing torsades des pointes in LQT2 and LQT3 models of the long-QT syndrome. *Circulation* 1997;96:2038–2047. doi: 10.1161/01.cir.96.6.2038
- Bos JM, Crotti L, Rohatgi RK, Castelletti S, Dagradi F, Schwartz PJ, Ackerman MJ. Mexiletine shortens the QT interval in patients with potassium channel-mediated type 2 long QT syndrome. *Circ Arrhythm Electrophysiol* 2019;12:e007280. doi: 10.1161/CIRCEP.118.007280
- Chorin E, Hu D, Antzelevitch C, Hochstadt A, Belardinelli L, Zeltser D, Barajas-Martinez H, Rozovski U, Rosso R, Adler A, et al. Ranolazine for congenital long-QT syndrome type III: experimental and long-term clinical data. *Circ Arrhythm Electrophysiol* 2016;9:e004370. doi: 10.1161/CIRCEP.116.004370
- Giustetto C, Schimpf R, Mazzanti A, Scrocco C, Maury P, Anttonen O, Probst V, Blanc JJ, Sbragia P, Dalmasso P, et al. Long-term follow-up of patients with short QT syndrome. *J Am Coll Cardiol* 2011;58:587–595. doi: 10.1016/j.jacc.2011.03.038
- Andorin A, Gourraud JB, Mansourati J, Fouchard S, le Marec H, Maury P, Mabo P, Hermida JS, Deharo JC, Delasalle B, et al. The QUIDAM study: hydroquinidine therapy for the management of Brugada syndrome patients at high arrhythmic risk. *Heart Rhythm* 2017;14:1147–1154. doi: 10.1016/j.hrthm.2017.04.019
- Chen-lzu Y, Izu LT, Hegyi B, Bányász T. Recording of ionic currents under physiological conditions: action potential-clamp and 'onion-peeling' techniques. In: Jue T, ed. *Modern Tools of Biophysics*. New York, NY: Springer New York; 2017:31–48.
- Hegyí B, Bossuyt J, Ginsburg KS, Mendoza LM, Talken L, Ferrier WT, Pogwizd SM, Izu LT, Chen-lzu Y, Bers DM. Altered repolarization reserve in failing rabbit ventricular myocytes: calcium and β -adrenergic effects on delayed- and inward-rectifier potassium currents. *Circ Arrhythm Electrophysiol* 2018;11:e005852. doi: 10.1161/CIRCEP.117.005852
- Piccirillo G, Magri D, Matera S, Magnanti M, Torrini A, Pasquazzi E, Schifano E, Velitti S, Marigliano V, Quaglione R, et al. QT variability strongly predicts sudden cardiac death in asymptomatic subjects with mild or moderate left ventricular systolic dysfunction: a prospective study. *Eur Heart J* 2007;28:1344–1350. doi: 10.1093/eurheartj/ehl367
- Hegyí B, Chen-lzu Y, Izu LT, Bányász T. Altered K+ current profiles underlie cardiac action potential shortening in hyperkalemia and β -adrenergic stimulation. *Can J Physiol Pharmacol* 2019;97:773–780. doi: 10.1139/cjpp-2019-0056
- Pogwizd SM, Schlotthauer K, Li L, Yuan W, Bers DM. Arrhythmogenesis and contractile dysfunction in heart failure: roles of sodium-calcium exchange, inward rectifier potassium current, and residual beta-adrenergic responsiveness. *Circ Res* 2001;88:1159–1167. doi: 10.1161/hh1101.091193
- Hegyí B, Morotti S, Liu C, Ginsburg KS, Bossuyt J, Belardinelli L, Izu LT, Chen-lzu Y, Bányász T, Grandi E, et al. Enhanced depolarization drive in failing rabbit ventricular myocytes: calcium-dependent and β -Adrenergic effects on late sodium, L-Type calcium, and sodium-calcium exchange currents. *Circ Arrhythm Electrophysiol* 2019;12:e007061. doi: 10.1161/CIRCEP.118.007061
- Szentandrassy N, Kistamás K, Hegyi B, Horváth B, Ruzsnavszky F, Váci K, Magyar J, Bányász T, Varró A, Nánási PP. Contribution of ion currents to beat-to-beat variability of action potential duration in canine ventricular myocytes. *Pflugers Arch* 2015;467:1431–1443. doi: 10.1007/s00042-014-1581-4
- Hegyí B, Horváth B, Váci K, Gónczi M, Kistamás K, Ruzsnavszky F, Veress R, Izu LT, Chen-lzu Y, Bányász T, et al. Ca2+-activated Cl- current is antiarrhythmic by reducing both spatial and temporal heterogeneity of cardiac repolarization. *J Mol Cell Cardiol* 2017;109:27–37. doi: 10.1016/j.jmcc.2017.06.014
- Ai X, Curran JW, Shannon TR, Bers DM, Pogwizd SM. Ca2+/calmodulin-dependent protein kinase modulates cardiac ryanodine receptor phosphorylation and sarcoplasmic reticulum Ca2+ leak in heart failure. *Circ Res* 2005;97:1314–1322. doi: 10.1161/01.RES.0000194329.41863.89
- Eichel CA, Rios-Perez EB, Liu F, Jameson MB, Jones DK, Knickelbine JJ, Robertson GA. A microtranslatome coordinately regulates sodium and potassium currents in the human heart. *eLife* 2019;8:e52654. doi: 10.7554/eLife.52654.
- Altomare C, Bartolucci C, Sala L, Bernardi J, Mostacciolo G, Rocchetti M, Severi S, Zaza A. IKr impact on repolarization and its variability assessed by dynamic clamp. *Circ Arrhythm Electrophysiol* 2015;8:1265–1275. doi: 10.1161/CIRCEP.114.002572
- Maltsev VA, Sabbah HN, Higgins RS, Silverman N, Lesch M, Undrovinas AI. Novel, ultraslow inactivating sodium current in human ventricular cardiomyocytes. *Circulation* 1998;98:2545–2552. doi: 10.1161/01.cir.98.23.2545
- Maltsev VA, Reznikov V, Undrovinas NA, Sabbah HN, Undrovinas A. Modulation of late sodium current by Ca2+, calmodulin, and CaMKII in normal and failing dog cardiomyocytes: similarities and differences. *Am J Physiol Heart Circ Physiol* 2008;294:H1597–H1608. doi: 10.1152/ajpheart.00484.2007
- Belardinelli L, Liu G, Smith-Maxwell C, Wang WQ, El-Bizri N, Hirakawa R, Karpinski S, Li CH, Hu L, Li XJ, et al. A novel, potent, and selective inhibitor of cardiac late sodium current suppresses experimental arrhythmias. *J Pharmacol Exp Ther* 2013;344:23–32. doi: 10.1124/jpet.112.198887
- Wagner S, Dybkova N, Rasenack EC, Jacobsen C, Fabritz L, Kirchhof P, Maier SK, Zhang T, Hasenfuss G, Brown JH, et al. Ca2+/calmodulin-dependent protein kinase II regulates cardiac Na+ channels. *J Clin Invest* 2006;116:3127–3138. doi: 10.1172/JCI26620
- Glynn P, Musa H, Wu X, Unudurthi SD, Little S, Qian L, Wright PJ, Radwanski PB, Gyorke S, Mohler PJ, et al. Voltage-Gated sodium channel phosphorylation at Ser571 regulates late current, arrhythmia, and cardiac function in vivo. *Circulation* 2015;132:567–577. doi: 10.1161/CIRCULATIONAHA.114.015218
- Hegyí B, Bányász T, Izu LT, Belardinelli L, Bers DM, Chen-lzu Y. β -adrenergic regulation of late Na+ current during cardiac action potential is mediated by both PKA and CaMKII. *J Mol Cell Cardiol* 2018;123:168–179. doi: 10.1016/j.jmcc.2018.09.006

34. Hegyi B, Komáromi I, Nánási PP, Szentandrassy N. Selectivity problems with drugs acting on cardiac Na^+ and Ca^{2+} channels. *Curr Med Chem*. 2013;20:2552–2571. doi: 10.2174/09298673113209990123
35. Haufe V, Cordeiro JM, Zimmer T, Wu YS, Schiccitano S, Benndorf K, Dumaine R. Contribution of neuronal sodium channels to the cardiac fast sodium current I_{Na} is greater in dog heart Purkinje fibers than in ventricles. *Cardiovasc Res*. 2005;65:117–127. doi: 10.1016/j.cardiores.2004.08.017
36. Hegyi B, Bárándi L, Komáromi I, Papp F, Horváth B, Magyar J, Bányász T, Krasznai Z, Szentandrassy N, Nánási PP. Tetrodotoxin blocks L-type Ca^{2+} channels in canine ventricular cardiomyocytes. *Pflugers Arch*. 2012;464:167–174. doi: 10.1007/s00424-012-1114-y
37. Koltun DO, Parkhill EQ, Elzein E, Kobayashi T, Notte GT, Kalla R, Jiang RH, Li X, Perry TD, Avila B, et al. Discovery of triazolopyridine GS-458967, a late sodium current inhibitor (Late I_{Na}) of the cardiac NaV 1.5 channel with improved efficacy and potency relative to ranolazine. *Bioorg Med Chem Lett*. 2016;26:3202–3206. doi: 10.1016/j.bmcl.2016.03.101
38. Bárándi L, Virág L, Jost N, Horváth Z, Koncz I, Papp R, Harmati G, Horváth B, Szentandrassy N, Bányász T, et al. Reverse rate-dependent changes are determined by baseline action potential duration in mammalian and human ventricular preparations. *Basic Res Cardiol*. 2010;105:315–323. doi: 10.1007/s00395-009-0082-7
39. Kornyevev D, El-Bizri N, Hirakawa R, Nguyen S, Viatchenko-Karpinski S, Yao L, Rajamani S, Belardinelli L. Contribution of the late sodium current to intracellular sodium and calcium overload in rabbit ventricular myocytes treated by anemone toxin. *Am J Physiol Heart Circ Physiol*. 2016;310:H426–H435. doi: 10.1152/ajpheart.00520.2015
40. Wasserstrom JA, Sharma R, O'Toole MJ, Zheng J, Kelly JE, Shryock J, Belardinelli L, Aistrup GL. Ranolazine antagonizes the effects of increased late sodium current on intracellular calcium cycling in rat isolated intact heart. *J Pharmacol Exp Ther*. 2009;331:382–391. doi: 10.1124/jpet.109.156471
41. Ke HY, Yang HY, Francis AJ, Collins TP, Surendran H, Alvarez-Laviada A, Firth JM, MacLeod KT. Changes in cellular Ca^{2+} and Na^+ regulation during the progression towards heart failure in the guinea pig. *J Physiol*. 2020;598:1339–1359. doi: 10.1113/JP277038
42. Nattel S, Maguy A, Le Bouter S, Yeh YH. Arrhythmogenic ion-channel remodeling in the heart: heart failure, myocardial infarction, and atrial fibrillation. *Physiol Rev*. 2007;87:425–456. doi: 10.1152/physrev.00014.2006
43. Gaita F, Giustetto C, Bianchi F, Schimpf R, Haissaguerre M, Calò L, Brugada R, Antzelevitch C, Borggrefe M, Wolpert C. Short QT syndrome: pharmacological treatment. *J Am Coll Cardiol*. 2004;43:1494–1499. doi: 10.1016/j.jacc.2004.02.034
44. Wu L, Rajamani S, Shryock JC, Li H, Ruskin J, Antzelevitch C, Belardinelli L. Augmentation of late sodium current unmasks the proarrhythmic effects of amiodarone. *Cardiovasc Res*. 2008;77:481–488. doi: 10.1093/cvr/cvm069
45. Antzelevitch C, Belardinelli L, Zygmunt AC, Burashnikov A, Di Diego JM, Fish JM, Cordeiro JM, Thomas G. Electrophysiological effects of ranolazine, a novel antiarrhythmic agent with antiarrhythmic properties. *Circulation*. 2004;110:904–910. doi: 10.1161/01.CIR.0000139333.83620.5D
46. Paul AA, Witchel HJ, Hancox JC. Inhibition of the current of heterologously expressed HERG potassium channels by flecainide and comparison with quinidine, propafenone and lignocaine. *Br J Pharmacol*. 2002;136:717–729. doi: 10.1038/sj.bjp.0704784
47. Yang PC, El-Bizri N, Romero L, Giles WR, Rajamani S, Belardinelli L, Clancy CE. A computational model predicts adjunctive pharmacotherapy for cardiac safety via selective inhibition of the late cardiac Na current. *J Mol Cell Cardiol*. 2016;99:151–161. doi: 10.1016/j.yjmcc.2016.08.011
48. Morita N, Lee JH, Xie Y, Sovari A, Qu Z, Weiss JN, Karagueuzian HS. Suppression of re-entrant and multifocal ventricular fibrillation by the late sodium current blocker ranolazine. *J Am Coll Cardiol*. 2011;57:366–375. doi: 10.1016/j.jacc.2010.07.045
49. Morotti S, Grandi E. Quantitative systems models illuminate arrhythmia mechanisms in heart failure: role of the Na^+ - Ca^{2+} - Ca^{2+} /calmodulin-dependent protein kinase II-reactive oxygen species feedback. *Wiley Interdiscip Rev Syst Biol Med*. 2019;11:e1434. doi: 10.1002/wsbm.1434
50. Hegyi B, Bers DM, Bossuyt J. $CaMKII$ signaling in heart diseases: emerging role in diabetic cardiomyopathy. *J Mol Cell Cardiol*. 2019;127:246–259. doi: 10.1016/j.yjmcc.2019.01.001
51. Studenik CR, Zhou Z, January CT. Differences in action potential and early afterdepolarization properties in LQT2 and LQT3 models of long QT syndrome. *Br J Pharmacol*. 2001;132:85–92. doi: 10.1038/sj.bjp.0703770
52. Horváth B, Hegyi B, Kistamás K, Váci K, Bányász T, Magyar J, Szentandrassy N, Nánási PP. Cytosolic calcium changes affect the incidence of early afterdepolarizations in canine ventricular myocytes. *Can J Physiol Pharmacol*. 2015;93:527–534. doi: 10.1139/cjpp-2014-0511
53. Tseng GN. $I(Kr)$: the hERG channel. *J Mol Cell Cardiol*. 2001;33:835–849. doi: 10.1006/jmcc.2000.1317
54. Xie Y, Grandi E, Puglisi JL, Sato D, Bers DM. β -adrenergic stimulation activates early afterdepolarizations transiently via kinetic mismatch of PKA targets. *J Mol Cell Cardiol*. 2013;58:153–161. doi: 10.1016/j.yjmcc.2013.02.009
55. Ruzsnavszky F, Hegyi B, Kistamás K, Váci K, Horváth B, Szentandrassy N, Bányász T, Nánási PP, Magyar J. Asynchronous activation of calcium and potassium currents by isoproterenol in canine ventricular myocytes. *Naunyn Schmiedeberg's Arch Pharmacol*. 2014;387:457–467. doi: 10.1007/s00210-014-0964-6
56. Szentmiklosi AJ, Szentandrassy N, Hegyi B, Horvath B, Magyar J, Bányász T, Nánási PP. Chemistry, physiology, and pharmacology of β -adrenergic mechanisms in the heart. Why are β -blocker antiarrhythmics superior? *Curr Pharm Des*. 2015;21:1030–1041. doi: 10.2174/1381612820666141029111240
57. Szentandrassy N, Farkas V, Bárándi L, Hegyi B, Ruzsnavszky F, Horváth B, Bányász T, Magyar J, Márton I, Nánási PP. Role of action potential configuration and the contribution of Ca^{2+} and K^+ currents to isoprenaline-induced changes in canine ventricular cells. *Br J Pharmacol*. 2012;167:599–611. doi: 10.1111/j.1476-5381.2012.02015.x
58. Ponce-Balbuena D, Guerrero-Serna G, Valdivia CR, Caballero R, Díez-Guerra FJ, Jiménez-Vázquez EN, Ramírez RJ, Monteiro da Rocha A, Herron TJ, Campbell KF, et al. Cardiac $Kir2.1$ and $NaV1.5$ channels traffic together to the sarcolemma to control excitability. *Circ Res*. 2018;122:1501–1516. doi: 10.1161/CIRCRESAHA.117.311872
59. Johnson DM, Heijman J, Bode EF, Greensmith DJ, van der Linde H, Abi-Gerges N, Eisner DA, Trafford AW, Volders PG. Diastolic spontaneous calcium release from the sarcoplasmic reticulum increases beat-to-beat variability of repolarization in canine ventricular myocytes after β -adrenergic stimulation. *Circ Res*. 2013;112:246–256. doi: 10.1161/CIRCRESAHA.112.275735
60. Kistamas K, Szentandrassy N, Hegyi B, Váci K, Ruzsnavszky F, Horvath B, Banyasz T, Nánási PP, Magyar J. Changes in intracellular calcium concentration influence beat-to-beat variability of action potential duration in canine ventricular myocytes. *J Physiol Pharmacol*. 2015;66:73–81.
61. Kim JJ, Némec J, Li Q, Salama G. Synchronous systolic subcellular Ca^{2+} -elevations underlie ventricular arrhythmia in drug-induced long QT type 2. *Circ Arrhythm Electrophysiol*. 2015;8:703–712. doi: 10.1161/CIRCEP.114.002214
62. Sala L, Gnechi M, Schwartz PJ. Long QT syndrome modelling with cardiomyocytes derived from human-induced pluripotent stem cells. *Arrhythm Electrophysiol Rev*. 2019;8:105–110. doi: 10.15420/aer.2019.1.1
63. Baczkó I, Jost N, Virág L, Bószé Z, Varró A. Rabbit models as tools for preclinical cardiac electrophysiological safety testing: importance of repolarization reserve. *Prog Biophys Mol Biol*. 2016;121:157–168. doi: 10.1016/j.pbiomolbio.2016.05.002

SUPPLEMENTAL MATERIAL

Supplemental Methods

Animal Models and Cardiomyocyte Isolation

Single cardiomyocytes from the midmyocardial region of the left ventricular free wall were isolated from sixteen young adult (4-month-old) male New Zealand White rabbits as previously described.¹ Briefly, in rabbits 15 minutes before terminal surgery heparin (400 U/kg) was injected, and then they were anesthetized with isoflurane (3 to 3.5%) inhalation. After achieving deep anesthesia, hearts were quickly excised and placed in a cold Tyrode solution. The hearts were mounted on a Langendorff apparatus and retrogradely perfused for 5 minutes with oxygenated Tyrode solution to remove blood from the coronary vasculature. Then the hearts were perfused with a Ca²⁺-free Tyrode solution for 3 minutes to stop the contraction of the heart. Next, this solution was supplemented with 1 mg/mL type II collagenase (Worthington, Lakewood, NJ, USA), 0.05 mg/mL protease type XIV (Sigma-Aldrich, St. Louis, MO, USA) and 50 μmol/L Ca²⁺, and the hearts were perfused for an additional 25 to 30 minutes to enzymatically dissociate the cells. After perfusion, both atria, the right ventricle, and the septum were removed, the left ventricle was minced, and ventricular cells were then harvested and stored in Tyrode solution.

The rabbit model of congestive heart failure (HF) induced by combined volume and pressure overload was used (detailed morphometric and echocardiography data are shown in Table I in the Data Supplement), and cardiomyocyte isolation from the failing and age-matched control (AM) hearts have been performed as previously described.^{2,3} Briefly, rabbits were subjected to general anesthesia (induction with 2 mg/kg propofol followed by 2 to 5% isoflurane in 100% oxygen). After thoracotomy, the heart was quickly excised and rinsed in cold nominally Ca²⁺-free Minimal Essential Medium. The right atrium was removed, and the aorta opened to visualize the left coronary ostium which was then cannulated using a 5F Judkins right catheter (Performa; Merit Medical Systems, South Jordan, UT, USA). Perfusion of the left ventricle and left atrium was established before removal of the right ventricular free wall and application of a purse-string suture to secure the catheter in place. The remainder of the isolation followed the previously described procedure.²

The porcine model of chronic myocardial infarction (MI) used in this study was developed to provide a clinically relevant large animal ischemic cardiomyopathy model.⁴ In six adult Yucatan mini-pigs (4- to 6-month-old, 45 to 60 kg) transmural MI was induced by targeted microbead embolization of the first diagonal branch of the left anterior descending (LAD) coronary artery via injection of 2 mL 90 μm diameter polystyrene micro-spheres (Polybead, Polysciences Inc., Warrington, PA, USA), resulting in significant left ventricular dysfunction and remodeling.^{4,5} These pigs were part of a larger study examining the complex electrophysiological remodeling in post-MI failing hearts,⁵ here we report a subset of those animals, focusing on I_{Kr} and I_{NaL} experiments. Five months after MI induction, the pigs were sacrificed under general inhalation anesthesia. Briefly, following thoracotomy, the heart was placed in a cardioplegic solution (containing in mmol/L: CaCl₂ 1.2, MgCl₂ 34.1, KCl 16, NaHCO₃ 10 and NaCl 110) *in situ* before excision. This was followed by perfusion with custodial HTK (histidine-tryptophan-ketoglutarate) solution (containing in mmol/L: NaCl 15, KCl 9, MgCl₂ 4, L-histidine hydrochloride 18, L-histidine 180, tryptophan 2, mannitol 30, CaCl₂ 0.015, and potassium hydrogen 2-ketoglutarate 2) supplemented with 10 mmol/L 2,3-butanedione monoxime (BDM). For functional cell studies, left ventricular cardiomyocytes from the remote zone of the infarct (or from the same location in age-matched sham control hearts) were obtained by enzymatic digestion using cannulation and perfusion of the left coronary vasculature (either coronary sinus or the left circumflex coronary artery) as previously described.⁵

Electrophysiology

Isolated single ventricular cardiomyocytes were placed in a temperature-controlled Plexiglas chamber (Cell Microsystems Inc., Research Triangle Park, NC, USA) and continuously perfused with a modified Tyrode solution containing (in mmol/L): NaCl 124, NaHCO₃ 25, KCl 4, CaCl₂ 1.2, MgCl₂ 1, HEPES 10, and

glucose 10; pH=7.40. Electrodes were fabricated from borosilicate glass (World Precision Instruments Inc., Sarasota, FL, USA) having tip resistances of 2 to 2.5 M Ω when filled with internal solution containing (in mmol/L): K-aspartate 110, KCl 25, NaCl 5, Mg-ATP 3, HEPES 10, cAMP 0.002, phosphocreatine dipotassium salt 10, and EGTA 0.01; pH=7.20. Using this internal solution preserves the Ca²⁺ transient and contraction of the cardiomyocyte.⁶ In a few experiments in HF and AM cells, the pipette solution was supplemented with 10 mmol/L BAPTA which buffers [Ca²⁺]_i to nominally zero.

Axopatch 200B amplifier (Axon Instruments Inc., Union City, CA, USA) was used for recordings and the signals were digitized at 50 kHz by a Digidata 1440A A/D converter (Molecular Devices, Sunnyvale, CA, USA). Series resistance was typically 3 to 5 M Ω and it was compensated by $\geq 80\%$. Experiments were discarded when the series resistance was high or increased by $\geq 20\%$ during the recordings. Reported voltages are already corrected for liquid junction potential. Experiments were conducted at 36 \pm 0.1 $^{\circ}$ C.

APs were recorded in whole-cell I-clamp conditions where cells were stimulated using supra-threshold depolarizing pulses (2 ms duration) delivered via the patch pipette.

Self AP-clamp experiments were conducted as previously described.^{5,7} Briefly, the cell's steady-state AP was recorded under I-clamp, and then it was used in the same cell as the voltage command under V-clamp at the same pacing frequency. In control, the net current output (reference or control current) should be zero after reaching equilibrium. Next, the current of interest is isolated by using its specific blocker to remove it from the net current output (compensation current). Then the drug-sensitive current is obtained by subtraction (difference current=reference current-compensation current). Applying additional specific blockers and repeating the recording steps, several ionic currents can be sequentially isolated from the same cell. Note that ionic currents were recorded after their specific blocker had reached steady-state effect (usually in 2 minutes using local perfusion). Ionic currents were dissected by using specific inhibitors in a sequence minimizing the off-target effects of a blocker on other ion channels, eg, nifedipine, blocker of L-type Ca²⁺ current (I_{CaL}) can be used only as a last step to preserve [Ca²⁺]_i transient and its influence on other ionic currents. The following sequence of selective blockers has been used for dissecting out a given ionic current: 1 μ mol/L GS-967 for I_{NaL}, 10 μ mol/L tetrodotoxin (TTX) for transient Na⁺ current (I_{NaT}), 1 μ mol/L E-4031 for I_{Kr}, 1 μ mol/L HMR-1556 for slow delayed rectifier K⁺ current (I_{Ks}), 100 nmol/L apamin for small conductance (SK) Ca²⁺-activated K⁺ current (I_{K(Ca)}), 100 μ mol/L BaCl₂ for inward rectifier K⁺ current (I_{K1}), 3 mmol/L 4-aminopyridine for transient outward K⁺ current (I_{to}), 100 μ mol/L CaCCinh-A01 for Ca²⁺-activated Cl⁻ current (I_{Cl(Ca)}), 500 nmol/L ORM-10962 for Na⁺/Ca²⁺ exchange current (I_{NCX}), and 10 μ mol/L nifedipine for L-type Ca²⁺ current (I_{CaL}) (see also Table II in the Data Supplement for drug selectivity data). Note that in this study (except for Figure 1) only the selective and potent inhibitors E-4031 and GS-967 have been used to systematically compare the profiles of I_{Kr} and I_{NaL}, respectively.

Ionic currents were normalized to cell capacitance measured in each cell using short (10 ms) hyperpolarizing pulses from -10 mV to -20 mV. The capacitance of ventricular cardiomyocytes was 144.7 \pm 1.7 pF (n/N=113 cells/20 animals) in control young adult rabbits. The cell capacitance was 173.7 \pm 3.8 pF (n/N=32 cells/6 animals) in HF versus 142.5 \pm 2.3 pF (n/N=31 cells/4 animals) in age-matched control rabbits ($P < 0.001$ using Student *t* test). Similar cellular hypertrophy was found in post-MI ischemic HF pigs (174.9 \pm 11.2 pF, n/N=13 cells/6 animals) versus age-matched sham control animals (145.3 \pm 4.2 pF, n/N=12 cells/5 animals, $P < 0.05$ using Student *t* test). To characterize each ionic current, we reported the current density (current magnitude/cell capacitance) and the net charge carried by each ionic current under AP-clamp (analyzed between 10 ms after the peak of the AP and APD₉₀).

	Age-matched Control	Heart Failure
Age (years)	2.28±0.16	2.24±0.48 ^{NS}
Body weight (kg)	4.01±0.18	4.19±0.18 ^{NS}
Heart weight (g)	10.98±0.38	23.42±2.19**
HW/BW (g/kg)	2.75±0.11	5.66±0.63**
Lung weight (g)	13.73±0.27	18.80±0.93*
LuW/BW (g/kg)	3.44±0.15	5.54±0.54 ^{P=0.10}
Liver weight (g)	68.17±6.79	82.22±8.85 ^{NS}
LiW/BW (g/kg)	17.34±0.80	19.95±2.64 ^{NS}
Kidney weight (g)	15.63±0.19	15.00±0.57 ^{NS}
KW/BW (g/kg)	4.02±0.18	3.59±0.10 ^{P=0.12}
LVEDD (cm)	1.54±0.13	2.35±0.11**
LVESD (cm)	1.06±0.08	1.88±0.16**
FS (%)	35.35±1.95	28.33±1.24*

Supplemental Table I. Morphometric and echocardiography data of heart failure and age-matched control rabbits.

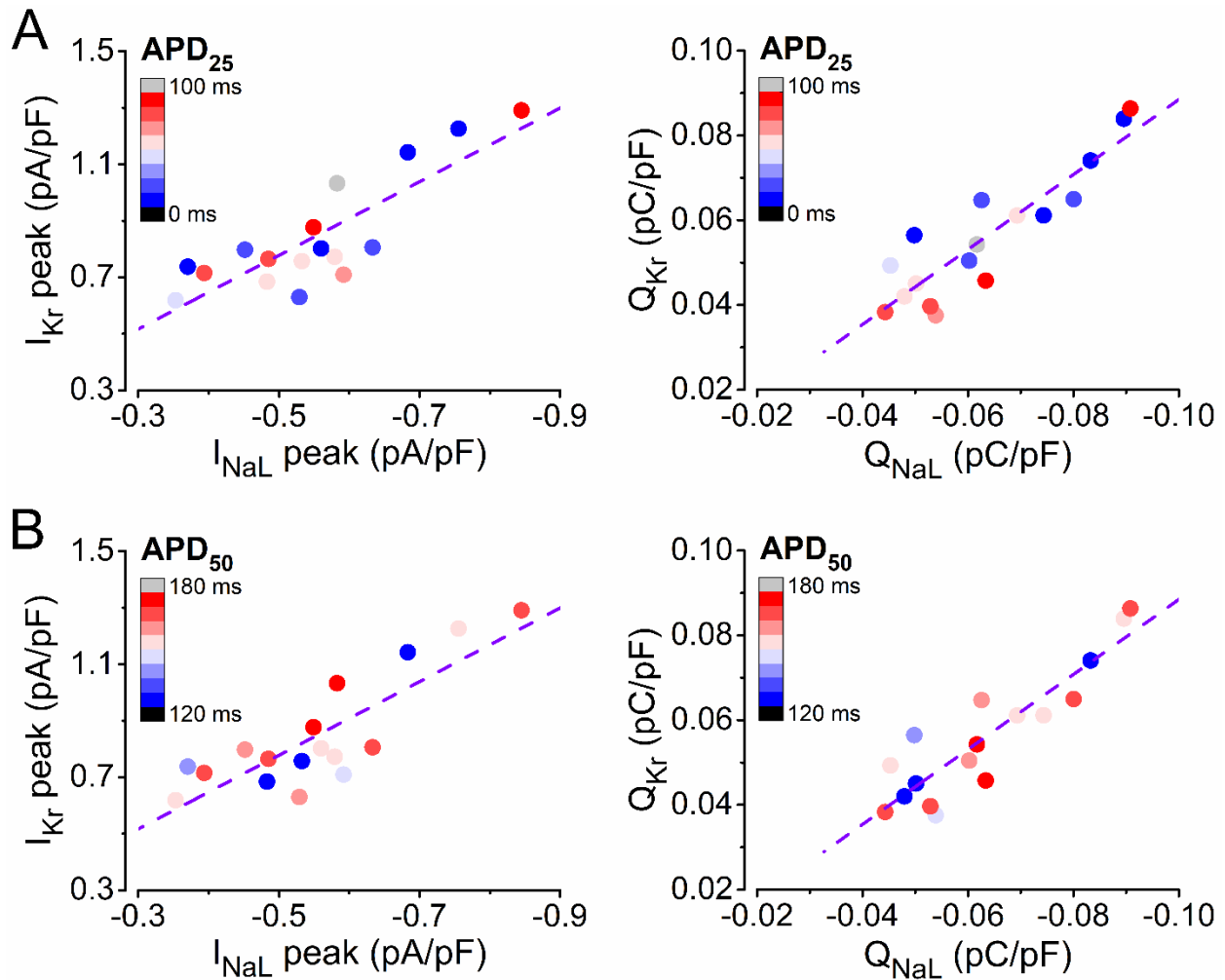
Heart failure (HF) was induced in 6 rabbits and progression was assessed periodically by echocardiography. Data of HF rabbits at the time when cardiomyocytes were isolated are compared with 4 age-matched healthy control rabbits. Increased heart weight and HW/BW demonstrate significant myocardial hypertrophy in HF. Increased lung weight indicates pulmonary congestion in HF. Enlarged left ventricular dimensions and fraction shortening measured in M-mode echocardiography demonstrate ventricular dilation and functional impairment in HF. All data represent mean±SEM. Student *t* test. *NS*, not significant ($P>0.05$), * $P<0.05$; ** $P<0.01$.

(HW/BW, heart weight-to-body weight ratio; LuW/BW, lung weight-to-body weight ratio; LiW/BW, liver weight-to-body weight ratio; KW/BW, kidney weight-to-body weight ratio; LVEDD, left ventricular end-diastolic diameter; LVESD, left ventricular end-systolic diameter; FS, fractional shortening, calculated as $FS=[LVEDD-LVESD]/LVEDD\times 100$.)

	Inhibitor	Dose	Reference
Late Na ⁺ current (I _{NaL})	GS-967	1 μmol/L	8, 9
Transient Na ⁺ current (I _{NaT})	Tetrodotoxin	10 μmol/L	10, 11
Rapid delayed rectifier K ⁺ current (I _{Kr})	E-4031	1 μmol/L	12, 13
Slow delayed rectifier K ⁺ current (I _{Ks})	HMR-1556	1 μmol/L	14, 15
Ca ²⁺ -activated K ⁺ current (I _{K(Ca)})	Apamin	100 nmol/L	16, 17
Inward rectifier K ⁺ current (I _{K1})	Ba ²⁺	100 μmol/L	18, 19
Transient outward K ⁺ current (I _{to})	4-aminopyridine	5 mmol/L	20, 21
Ca ²⁺ -activated Cl ⁻ current (I _{Cl(Ca)})	CaCCinh-A01	30 μmol/L	22, 23
Na ⁺ /Ca ²⁺ exchanger current (I _{NCX})	ORM-10962	500 nmol/L	24, 25
L-type Ca ²⁺ current (I _{CaL})	Nifedipine	10 μmol/L	26, 27

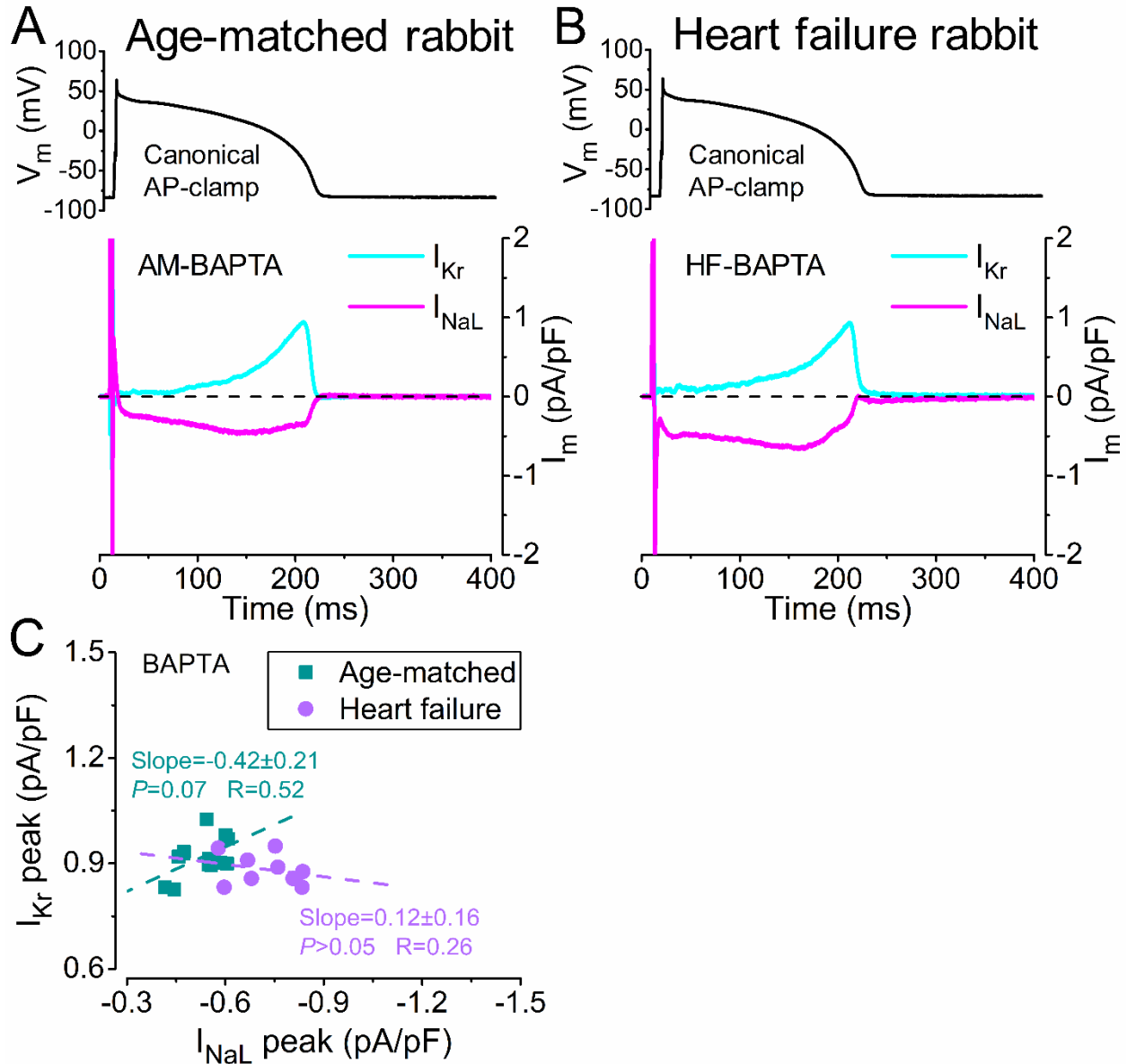
Supplemental Table II. Inhibitors used to measure specific drug-sensitive ionic currents under action potential (AP)-clamp.

List of drugs in the order of application in self AP-clamp sequential dissection experiment shown in Figure 1. These drugs are potent and selective inhibitors of each specific ion channels in the applied dosage (see *Supplemental References* for details).



Supplemental Figure I. Action potential repolarization timecourse and correlation between Q_{Kr} and Q_{NaL} in individual rabbit ventricular myocytes.

A, Action potential duration at 25% of repolarization (APD_{25}) of each control rabbit ventricular myocyte is color coded in the correlation plot between I_{Kr} and I_{NaL} peak densities and net charges. **B**, Action potential duration at 50% repolarization (APD_{50}) of each myocyte is color coded. Dashed lines represent the fitted linear regression curves.



Supplemental Figure II. I_{Kr} and I_{NaL} in heart failure under action potential (AP)-clamp with buffered $[Ca^{2+}]_i$.

A and **B**, Rapid delayed rectifier K^+ current (I_{Kr}) and late Na^+ current (I_{NaL}) in heart failure (HF) and age-matched control (AM) rabbits under canonical AP-clamp. I_{NaL} and I_{Kr} were measured as $1 \mu\text{mol/L}$ GS-967 and $1 \mu\text{mol/L}$ E-4031-sensitive currents under AP-clamp, respectively. 10 mmol/L BAPTA was used in the pipette to eliminate Ca^{2+} transient (BAPTA). Cells were paced at 2 Hz . **C**, Correlation between I_{Kr} and I_{NaL} peak densities in HF and AM measured with BAPTA. Dashed lines represent the fitted linear regression curves. $n/N=9$ cells/3 animals for both AM and HF.

SUPPLEMENTAL REFERENCES

1. Hegyi B, Chen-Izu Y, Izu LT and Banyasz T. Altered K⁺ current profiles underlie cardiac action potential shortening in hyperkalemia and beta-adrenergic stimulation. *Can J Physiol Pharmacol*. 2019;97:773-780. doi: 10.1139/cjpp-2019-0056.
2. Hegyi B, Bossuyt J, Ginsburg KS, Mendoza LM, Talken L, Ferrier WT, Pogwizd SM, Izu LT, Chen-Izu Y and Bers DM. Altered Repolarization Reserve in Failing Rabbit Ventricular Myocytes: Calcium and beta-Adrenergic Effects on Delayed- and Inward-Rectifier Potassium Currents. *Circ Arrhythm Electrophysiol*. 2018;11:e005852. doi: 10.1161/CIRCEP.117.005852.
3. Hegyi B, Morotti S, Liu C, Ginsburg KS, Bossuyt J, Belardinelli L, Izu LT, Chen-Izu Y, Banyasz T, Grandi E and Bers DM. Enhanced Depolarization Drive in Failing Rabbit Ventricular Myocytes. *Circ Arrhythm Electrophysiol*. 2019;12:e007061. doi: 10.1161/CIRCEP.118.007061.
4. Hanes DW, Wong ML, Jenny Chang CW, Humphrey S, Grayson JK, Boyd WD and Griffiths LG. Embolization of the first diagonal branch of the left anterior descending coronary artery as a porcine model of chronic trans-mural myocardial infarction. *J Transl Med*. 2015;13:187. doi: 10.1186/s12967-015-0547-4.
5. Hegyi B, Bossuyt J, Griffiths LG, Shimkunas R, Coulibaly Z, Jian Z, Grimsrud KN, Sondergaard CS, Ginsburg KS, Chiamvimonvat N, Belardinelli L, Varro A, Papp JG, Pollesello P, Levijoki J, Izu LT, Boyd WD, Banyasz T, Bers DM and Chen-Izu Y. Complex electrophysiological remodeling in postinfarction ischemic heart failure. *Proc Natl Acad Sci U S A*. 2018;115:E3036-E3044. doi: 10.1073/pnas.1718211115.
6. Horvath B, Banyasz T, Jian Z, Hegyi B, Kistamas K, Nanasi PP, Izu LT and Chen-Izu Y. Dynamics of the late Na(+) current during cardiac action potential and its contribution to afterdepolarizations. *J Mol Cell Cardiol*. 2013;64:59-68. doi: 10.1016/j.yjmcc.2013.08.010.
7. Chen-Izu Y, Izu LT, Hegyi B and Bányász T. Recording of Ionic Currents Under Physiological Conditions: Action Potential-Clamp and ‘Onion-Peeling’ Techniques. In: T. Jue, ed. *Modern Tools of Biophysics* New York, NY: Springer New York; 2017: 31-48. doi: 10.1007/978-1-4939-6713-1_2.
8. Belardinelli L, Liu G, Smith-Maxwell C, Wang WQ, El-Bizri N, Hirakawa R, Karpinski S, Li CH, Hu L, Li XJ, Crumb W, Wu L, Koltun D, Zablocki J, Yao L, Dhalla AK, Rajamani S and Shryock JC. A novel, potent, and selective inhibitor of cardiac late sodium current suppresses experimental arrhythmias. *J Pharmacol Exp Ther*. 2013;344:23-32. doi: 10.1124/jpet.112.198887.
9. Koltun DO, Parkhill EQ, Elzein E, Kobayashi T, Notte GT, Kalla R, Jiang RH, Li X, Perry TD, Avila B, Wang WQ, Smith-Maxwell C, Dhalla AK, Rajamani S, Stafford B, Tang J, Mollova N, Belardinelli L and Zablocki JA. Discovery of triazolopyridine GS-458967, a late sodium current inhibitor (Late INai) of the cardiac NaV 1.5 channel with improved efficacy and potency relative to ranolazine. *Bioorg Med Chem Lett*. 2016;26:3202-6. doi: 10.1016/j.bmcl.2016.03.101.
10. Satin J, Kyle JW, Chen M, Bell P, Cribbs LL, Fozzard HA and Rogart RB. A mutant of TTX-resistant cardiac sodium channels with TTX-sensitive properties. *Science*. 1992;256:1202-5. doi: 10.1126/science.256.5060.1202.
11. Hegyi B, Banyasz T, Izu LT, Belardinelli L, Bers DM and Chen-Izu Y. β -adrenergic regulation of late Na⁺ current during cardiac action potential is mediated by both PKA and CaMKII. *J Mol Cell Cardiol*. 2018;123:168-179. doi: 10.1016/j.yjmcc.2018.09.006.
12. Wettwer E, Scholtysik G, Schaad A, Himmel H and Ravens U. Effects of the new class III antiarrhythmic drug E-4031 on myocardial contractility and electrophysiological parameters. *J Cardiovasc Pharmacol*. 1991;17:480-7. doi: 10.1097/00005344-199103000-00018.
13. Liu DW and Antzelevitch C. Characteristics of the Delayed Rectifier Current (IKr and IKs) in Canine Ventricular Epicardial, Midmyocardial, and Endocardial Myocytes - a Weaker IKs Contributes to the Longer Action-Potential of the M-Cell. *Circ Res*. 1995;76:351-365. doi: 10.1161/01.res.76.3.351.
14. Gerlach U, Brendel J, Lang HJ, Paulus EF, Weidmann K, Bruggemann A, Busch AE, Suessbrich H, Bleich M and Greger R. Synthesis and activity of novel and selective I(Ks)-channel blockers. *J Med Chem*. 2001;44:3831-7. doi: 10.1021/jm0109255.

15. Thomas GP, Gerlach U and Antzelevitch C. HMR 1556, a potent and selective blocker of slowly activating delayed rectifier potassium current. *J Cardiovasc Pharmacol*. 2003;41:140-7. doi: 10.1097/00005344-200301000-00018.
16. Adelman JP, Maylie J and Sah P. Small-Conductance Ca²⁺-Activated K⁺ Channels: Form and Function. In: D. Julius and D. E. Clapham, eds. *Annu Rev Physiol, Vol 74*; 2012(74): 245-269. doi: 10.1146/annurev-physiol-020911-153336
17. Yu CC, Ai T, Weiss JN and Chen PS. Apamin does not inhibit human cardiac Na⁺ current, L-type Ca²⁺ current or other major K⁺ currents. *PLoS One*. 2014;9:e96691. doi: 10.1371/journal.pone.0096691.
18. Alagem N, Dvir M and Reuveny E. Mechanism of Ba²⁺ block of a mouse inwardly rectifying K⁺ channel: differential contribution by two discrete residues. *J Physiol*. 2001;534:381-393. doi: 10.1111/j.1469-7793.2001.00381.x.
19. Zaza A, Rocchetti M, Brioschi A, Cantadori A and Ferroni A. Dynamic Ca²⁺-induced inward rectification of K⁺ current during the ventricular action potential. *Circ Res*. 1998;82:947-56. doi: 10.1161/01.res.82.9.947.
20. Hiraoka M and Kawano S. Calcium-sensitive and insensitive transient outward current in rabbit ventricular myocytes. *J Physiol*. 1989;410:187-212. doi: 10.1113/jphysiol.1989.sp017528.
21. Nattel S, Matthews C, De Blasio E, Han W, Li D and Yue L. Dose-dependence of 4-aminopyridine plasma concentrations and electrophysiological effects in dogs : potential relevance to ionic mechanisms in vivo. *Circulation*. 2000;101:1179-84. doi: 10.1161/01.cir.101.10.1179.
22. Liu Y, Zhang H, Huang D, Qi J, Xu J, Gao H, Du X, Gamper N and Zhang H. Characterization of the effects of Cl⁻ channel modulators on TMEM16A and bestrophin-1 Ca²⁺ activated Cl⁻ channels. *Pflugers Arch*. 2015;467:1417-30. doi: 10.1007/s00424-014-1572-5.
23. Hegyi B, Horvath B, Vaczi K, Gonczi M, Kistamas K, Ruzsnavszky F, Veress R, Izu LT, Chen-Izu Y, Banyasz T, Magyar J, Csernoch L, Nanasi PP and Szentandrassy N. Ca²⁺-activated Cl⁻ current is antiarrhythmic by reducing both spatial and temporal heterogeneity of cardiac repolarization. *J Mol Cell Cardiol*. 2017;109:27-37. doi: 10.1016/j.yjmcc.2017.06.014.
24. Kohajda Z, Farkas-Morvay N, Jost N, Nagy N, Geramipour A, Horvath A, Varga RS, Hornyik T, Corici C, Acsai K, Horvath B, Prorok J, Ordog B, Deri S, Toth D, Levijoki J, Pollesello P, Koskelainen T, Otsomaa L, Toth A, Baczkó I, Lepran I, Nanasi PP, Papp JG, Varro A and Virag L. The Effect of a Novel Highly Selective Inhibitor of the Sodium/Calcium Exchanger (NCX) on Cardiac Arrhythmias in In Vitro and In Vivo Experiments. *PLoS One*. 2016;11:e0166041. doi: 10.1371/journal.pone.0166041.
25. Oravec K, Kormos A, Gruber A, Marton Z, Kohajda Z, Mirzaei L, Jost N, Levijoki J, Pollesello P, Koskelainen T, Otsomaa L, Toth A, Papp JG, Nanasi PP, Antoons G, Varro A, Acsai K and Nagy N. Inotropic effect of NCX inhibition depends on the relative activity of the reverse NCX assessed by a novel inhibitor ORM-10962 on canine ventricular myocytes. *Eur J Pharmacol*. 2018;818:278-286. doi: 10.1016/j.ejphar.2017.10.039.
26. Charnet P, Ouadid H, Richard S and Nargeot J. Electrophysiological analysis of the action of nifedipine and nifedipine on myocardial fibers. *Fundam Clin Pharmacol*. 1987;1:413-31. doi: 10.1111/j.1472-8206.1987.tb00575.x.
27. Shen JB, Jiang B and Pappano AJ. Comparison of L-type calcium channel blockade by nifedipine and/or cadmium in guinea pig ventricular myocytes. *J Pharmacol Exp Ther*. 2000;294:562-570.